The YAP1 isoform, YAP1-2α, promotes oncogenic properties by inducing liquid-liquid phase separation through specific heterodimerization with TAZ

Takuya Ooki[1], Takeru Hayashi[1], Yui Yamamoto[1], & Masanori Hatakeyama[1,2,*]

[1]Laboratory of Microbial Carcinogenesis, Institute of Microbial Chemistry, Microbial Chemistry Research Foundation, Tokyo, Japan

[2]Center of Infection-associated Cancer, Institute for Genetic Medicine, Hokkaido University, Sapporo, Japan

***e-mail: mhata@m.u-tokyo.ac.jp**

Running title

Molecular Mechanism of LLPS Induction by YAP isoform YAP1-2α

Keywords

Liquid-liquid phase separation, Cancer biology, Hippo pathway, alternative splicing, epithelial-mesenchymal transition (EMT), Ovarian cancer.

Abstract

The role of alternative splicing in initiating and promoting neoplastic transformation of cells poses a significant challenge in understanding cancer. The pro-oncogenic transcriptional coactivator YAP1 comprises at least eight isoforms, but their specific and overlapping functions in cancer development remain poorly understood. Here, we show that the YAP1-2 isoform, YAP1-2α, demonstrates significantly greater activity in inducing nuclear condensates through liquid-liquid phase separation (LLPS) compared to other isoforms. Mechanistically, YAP1-2α interacts specifically with its homologue TAZ via the leucine zipper, as well as with TEADs, which are the prevalent transcriptional partners of YAP1 and TAZ. The tetrameric complex is further assembled multivalently by BRD4 to promote LLPS formation. The resulting YAP1-2α/TAZ/TEAD complex binds to super-enhancer elements and strongly enhances pro-oncogenic target gene expression in a BRD4-dependent way. Cancer cells with higher YAP1-2α levels display a clear EMT signature that drives greater malignant traits. Similarly, increased YAP1-2α levels boost pro-oncogenic features such as sphere formation, invasion of the extracellular matrix, and resistance to various stresses, including anti-cancer drugs. In high-grade serous ovarian cancers (HGSOCs), higher YAP1-2α mRNA levels are characterized by nuclear YAP1 biomolecular condensates and associated with more advanced clinical stages. Our study shows that

YAP1-2α enhances cancer cell aggressiveness through LLPS formation, suggesting that the LLPS-induced YAP1-2α/TAZ/TEAD super-enhancer is a promising target for treating refractory cancers.

Introduction

Alternative splicing is a process in which a single gene produces multiple protein products, and its abnormalities are common in the progression of malignant tumors. Abnormal splicing affects key features of cancer, including cell growth, apoptosis, invasion, metastasis, drug resistance, and the immune response (1-3). Therefore, studying protein polymorphisms and their functions through alternative splicing during malignant progression may lead to the identification of promising cancer therapeutic targets.

YAP1 and its homologue TAZ lack a DNA-binding domain; instead, they activate downstream transcription by interacting with sequence-specific transcription factors, most notably the TEAD family transcription factors (TEAD1-4) (4, 5). The YAP1/TEAD and TAZ/TEAD complexes integrate signals related to mechanical, metabolic, and cell density to coordinate cell proliferation and differentiation during development and neoplastic progression by activating classical and super-enhancers (6, 7). In cancer cells, elevated levels of YAP1 and TAZ promote cancer stem-like properties by activating epithelial-to-mesenchymal transition (EMT)-inducing transcriptional regulators such as ZEB1 and SNAI2 through TEAD-dependent transactivation (8). Additionally, YAP1 and TAZ contribute to the acquisition of resistance to anticancer drugs (9). In particular, the transcriptional programs mediated by YAP1 and TAZ intersect with the KRAS-ERK MAPK pathway, sharing target genes that confer resistance to RAF and MEK inhibitors in various cancer cells (10,

11). While YAP1 and TAZ collaborate to control gene expression, their binding sites are not always identical or overlapping (12, 13). One possible reason for these differences may be related to splicing variants. Unlike TAZ, YAP1 pre-mRNA undergoes complex differential splicing, resulting in the production of at least eight YAP1 isoforms in human cells (14, 15). Indeed, these isoforms demonstrate both common and unique functions and regulate distinct sets of genes (16). However, the molecular mechanism by which structural variations in these YAP1 isoforms differentially regulate downstream genes remains unknown.

The presence or absence of exon 4, which encodes the second WW domain (WW 2), classifies YAP1 into YAP1-1 (with one WW domain) and YAP1-2 (with two WW domains). The WW domain binds proline-rich sequences like PPxY (17) and is crucial for nuclear translocation (18). There are four additional pre-mRNA splicing variants for both YAP1-1 and YAP1-2 forms. YAP1-1γ and YAP1-2γ mRNAs contain a shorter exon 5 (exon 5.1, missing the β-segment) and exon 6. YAP1-1δ and YAP1-2δ mRNAs feature a longer exon 5 (exon 5.2, including the β-segment) and exon 6 (which encodes the γ-segment). YAP1-1β and YAP1-2β mRNAs have exon 5.2 but lack exon 6, while YAP1-1α and YAP1-2α mRNAs include exon 5.1 but do not have exon 6. YAP1 isoforms can heterodimerize with TAZ via leucine zippers (19). However, the effects of these differences on cancer progression and the mechanisms behind them remain largely unexplored. In this work, we show that heterodimerization

of YAP1-2α with TAZ via a leucine zipper triggers liquid-liquid phase separation (LLPS). LLPS is a widespread phenomenon that supports the formation of membrane-less organelles, also known as biomolecular condensates, within cells. These organelles serve as sites for various bioreactions that regulate cellular functions (20, 21). Specifically, LLPS-mediated biomolecular condensation of transcription factors and coactivators within the nucleus is essential for the formation and activation of super-enhancers (22).

Super-enhancers are characterized by high concentrations of transcription factors, coactivators, mediators, and epigenetic modifiers that strongly enhance transcriptional output and integrate multiple signaling pathways that determine cell identity and state (23, 24). Cancer cells adapt to external environments by extensively rewiring their transcriptional networks through super-enhancer formation, which promotes malignant properties by supporting abnormal proliferation signaling, activating anti-apoptotic mechanisms, and facilitating invasion and metastasis. This process enables cancer cells to develop resistance to adverse conditions while also creating a tumor-favorable microenvironment, including an immunosuppressive state (25-29). We also demonstrate that YAP1-2α/TAZ-induced LLPS activates TEAD-specific super-enhancers, leading to increased expression of EMT-related genes and promoting the development of cancer hallmarks such as sphere formation, invasion, and resistance to various stresses, including drugs. This study uncovers the unexpected link between YAP1 splicing isoforms,

LLPS induction, and the activation of super-enhancers that contribute to malignant properties. Inhibition of splicing that generates YAP1-2α or disruption of the YAP1-2α/TAZ/TEAD complex may subvert malignant progression of cancer.

Results

YAP1 induces LLPS in a splicing variation-dependent manner

To elucidate the biological differences among YAP1 isoforms, we first generated *YAP1*-knockout (KO) UWB1.289 human high-grade serous ovarian cancer (HGSOC) cells using the CRISPR-Cas9 system. Immunoblot analysis confirmed the absence of endogenous YAP1-1 and YAP1-2 isoforms in the *YAP1*-KO cells (Fig. S1*A*, *lane 2*). These *YAP1*-KO cells were subsequently transfected with an expression vector for one of the four YAP1-2 isoforms fused with mVenus. The expression levels of the mVenus-fused YAP1-2 isoforms were comparable (Fig. S1*A*, *lanes 3-6*). We found greater nuclear puncta formation in cells expressing mVenus-fused YAP1-2α than other YAP1 isoforms (Fig. 1, *A-B*, Fig. S1*B*). To exclude the possibility that the puncta formation was due to the overexpression of mVenus-fused YAP1-2α, we also established *YAP1*-KO UWB1.289 cells reconstituted with HA-tagged YAP1-2α or YAP1-2γ at levels comparable to those of endogenous YAP1 (Fig. S1*C*). Immunofluorescence analysis using an anti-YAP1 antibody revealed that nuclear YAP1 puncta were present in YAP1-2α-reconstituted cells but absent in YAP1-2γ-reconstituted cells (Fig. 1*C*). This finding indicates that YAP1-2α specifically induces puncta formation in the nucleus. The formation of condensates of transcription cofactors within the nucleus is known to alter transcriptional activity by activating super-enhancers via LLPS formation (22-24). Biomolecular condensates formed via LLPS are

membrane-less and exhibit liquid-like properties such as droplet fusion and high molecular mobility within the droplet. These properties can be detected via fluorescence live cell imaging and Fluorescence Recovery After Photobleaching (FRAP) analysis (30). To further elucidate whether YAP1-2α puncta have liquid-like properties or not, we conducted time-lapse imaging experiment and FRAP analysis in *YAP1*-KO UWB1.289 cells transfected with mVenus-fused YAP1-2α. Administration of 1,6-hexanediol (Hex), an agent that disrupts liquid-like condensates without affecting solid aggregates, to mVenus-fused YAP1-2α-expressing cells eliminated puncta formation (Fig. 1*D*). In addition to this, YAP1-2α puncta exhibited puncta fusion (Fig. 1, *E*), and FRAP analysis revealed that they also form membrane-less puncta (Fig. 1, *F*-*G*, Fig. S1, *D*-*G*). Based on these observations, we concluded that YAP1-2α is a YAP1-2 splicing isoform capable of efficiently inducing LLPS in the nucleus.

YAP1-2α/TAZ/TEAD complex is required for LLPS formation

A previous study showed that the leucine zipper in the coiled-coil region of YAP1-2α interacts with the leucine zipper in TAZ's coiled-coil domain, forming a YAP1/TAZ heterodimer (19). Indeed, fluorescence imaging analysis demonstrated that TAZ colocalizes with YAP1-2α puncta (Fig. 2*A*). To determine if the leucine zipper structure of YAP1-2α is crucial for LLPS-induced puncta formation, we created a YAP1-2α leucine zipper mutant (LZM) by substituting the conserved leucine residues with alanine,

disrupting its structure. The disruption significantly reduced TEAD reporter activation by YAP1-2α (Fig. S2*A*). Expressing mVenus-fused YAP1-2α(LZM) in *YAP1*-KO UWB1.289 cells or MDA-MB-436 human triple-negative breast cancer (TNBC) cells markedly decreased puncta formation (Fig. 2*B*, Fig. S2, *B*-*C*). A proximity ligation assay (PLA) examined YAP1-2α and TAZ heterodimerization, revealing the TAZ formed a heterodimer with YAP1-2α(S94A) but not with YAP1-2α(LZM), YAP1-2α(LZM|S94A), or YAP1-2γ in the nucleus (Fig. S2*D*, upper). As expected, YAP1-2α, YAP1-2α(LZM), and YAP1-2γ interacted with TEAD, while YAP1-2α(S94A) and YAP1-2α(LZM|S94A) did not (Fig. S2*D*, lower). Moreover, YAP1-2α-induced LLPS puncta were eliminated by knocking out endogenous TAZ (Fig. 2*C*, Fig. S2*E*) or by shRNA-mediated inhibition of TAZ expression (Fig. S2*F*). Reciprocally, artificial heterodimerization between YAP1-2α(LZM) or YAP1-2γ and TAZ(LZM) promoted YAP1 puncta formation even with YAP1-2γ (Fig. 2, *D*-*E*, Fig. S2, *G*-*H*), confirming the essential role of YAP1-2α/TAZ heterodimerization in YAP1-2α-mediated LLPS induction.

To determine if TEADs (TEAD1-4), the critical partners of YAP1-2α and TAZ in promoter activation, are necessary for LLPS-mediated nuclear puncta formation, we expressed mVenus-fused YAP1-2α (wild-type, LZM, S94A) in UWB1.289 cells. Immunofluorescence staining indicated that TEAD and wild-type YAP1-2α colocalized within nuclear puncta but not the LZM or S94A mutant (Fig. 2*F*). Moreover, K-975, a selective inhibitor

of the interaction between TEAD and YAP1 or TAZ (31), eliminated LLPS puncta induced by YAP1-2α (Fig. 2*G*, Fig. S2*I*). Thus, YAP1-2α-induced nuclear condensates contained YAP1-2α, TAZ, and TEAD complexes. In this regard, YAP1-2α(S94A) also formed small puncta independently of TEAD, albeit slightly (Fig. 2, *F*-*G*), suggesting potential TEAD-independent mechanisms for weak condensate formation by YAP1-2α.

TAZ also forms a homodimer via the leucine zipper, leading to LLPS independently of YAP1 and TEAD (32). In contrast, YAP1 cannot form homodimers (19). TAZ/TAZ-LLPS condensates were similarly produced in both parental and *YAP1*-KO cells (Fig. S2*J*). PLA was used to visualize the interaction between TEAD and HA-tagged YAP1-2α or TAZ. This technique allowed us to distinguish between YAP1-2α/TAZ-LLPS condensates and TAZ/TAZ-LLPS condensates (Fig. S2*K*). Most YAP1-2α-TEAD complexes were localized within YAP1-2α/TAZ-induced LLPS condensates (Fig. S2*K*, right), whereas TAZ-TEAD complexes were located mostly outside TAZ/TAZ-induced LLPS condensates (Fig. S2*K*, left). This indicates the essential requirement of TEAD in YAP1-2α/TAZ -LLPS, while TAZ/TAZ-induced puncta likely contain other transcription factors. Indeed, TAZ/TAZ homodimers were present in TAZ/TAZ-LLPS but absent in YAP1-2α/TAZ-LLPS (Fig. 2*H*). These findings demonstrate that YAP1-2α/TAZ-LLPS is distinct from TAZ/TAZ-LLPS, the former being formed by YAP1-2α, TAZ, and TEAD complex (YAP1-2α/TAZ/TEAD-LLPS), and the latter by TAZ homodimer without YAP1

and TEAD (TAZ/TAZ-LLPS).

Mechanism of LLPS induction by YAP1-2α/TAZ/TEAD complex formation

YAP1-1 mRNA expression is significantly lower than *YAP1-2* mRNA in various cell types, especially cancer cells (33). Actually, the YAP1-2 protein is the dominant isoform in UWB1.289 cells, as shown in Figure S1*A*. The YAP1-1α isoform possesses a single WW domain and a functional leucine zipper in its coiled-coil domain, allowing it to heterodimerize with TAZ via the leucine zipper (Fig. S3*A*). To investigate if YAP1-1α induces LLPS, we expressed YAP1-1α or YAP1-2α in UWB1.289 cells. YAP1-1α produced fewer nuclear puncta than YAP1-2α, indicating it is significantly less effective in promoting LLPS induction (Fig. 3*A*, Fig. S3*B*).

The WW domain is a protein motif that preferentially interacts with proline-containing sequences such as PPxY and LPxY motifs (17, 34). LLPS enables the formation of membrane-less puncta or droplets in which specific proteins are concentrated via multivalent interactions (35). Nuclear puncta/condensates formed via LLPS, including transcription factors, coactivators, and mediators like BRD4 and MED1, are linked to super-enhancer formation. Thus, the presence of BRD4 in nuclear LLPS condensates indicates the potential for super-enhancers formation (36). Mediators are crucial in various transcription aspects, including linking transcription factors to RNA polymerase II (Pol II) (37). The role of BRD4

in LLPS relies on two bromodomains binding to H3K27ac, a marker of active enhancers (38). Since BRD4 contains an LPxY motif (LPDY) in bromodomain I and a PPxY motif (PPTY) in its C-terminal proline-rich region (Fig. 3*B*), we hypothesized these motifs interact with the two WW domains of YAP1-2α to facilitate multivalent protein interactions. Protein-protein interaction modeling using AlphaFold2 predicted that YAP1-2α's WW domains (WW1 and WW2) interact with BRD4's PPxY and LPxY motifs (Fig. 3*C*, Fig. S3*C*). Co-immunoprecipitation confirmed YAP1-2α and BRD4 interaction. This interaction was weakened when either PPxY or LPxY motif in BRD4 was disrupted and abolished when both were disrupted (Fig. 3*D*). The significance of BRD4 in YAP1-2α/TAZ/TEAD-LLPS condensates was verified by the results that shRNA-mediated BRD4 knockdown (Fig. 3*E*) and competitive inhibition of YAP1-BRD4 interaction (Fig. S3, *D-E*) abolished puncta formation. The reduction in YAP1-2α/TAZ/TEAD-LLPS puncta due to BRD4 knockdown was rescued by ectopic expression of shRNA-resistant wild-type BRD4, but not by BRD4 lacking one or both PPxY/LPxY motifs (Fig. 3*F*, Fig. S3*F*). Furthermore, results from reciprocal experiments introducing point mutations into either or both WW domain (s) of YAP1-2α revealed that loss of function in just one WW domain significantly reduced its binding capacity to BRD4 and drastically diminished YAP1-2α puncta formation (Fig. 3, *G-H*, Fig. S3, *G-H*). These findings indicate that the interactions between BRD4's PPxY/LPxY motif and YAP1's WW domains are crucial

for generating YAP1-2α/TAZ/TEAD-induced LLPS condensates.

YAP1-2α/TAZ/TEAD complex binds to TEAD-positive super-enhancer elements and reinforces gene expression

To investigate whether LLPS formation via heterodimerization of YAP1-2α and TAZ effects gene expression, we first confirmed typical TEAD target gene, *CCN1* (*Cyr61*) and *CCN2* (*CTGF*), expression levels in YAP1-2 isoforms transfected UWB1.289 cells. YAP1-2 isoforms increased *CCN2* mRNA expression to a similar degree (Fig. S4, *A-B*), whereas YAP1-2α significantly elevated *CCN1* mRNA expression compared to other isoforms (Fig. 4*A*). This increased *CCN1* was suppressed by TAZ knockout but not increased *CCN2* (Fig. 4*B*, Fig. S4, *C-D*). Conversely, inducing artificial YAP1/TAZ heterodimerization as indicated Figure 2*E* enhanced *CCN1* gene expression (Fig. 4*C*), indicating that YAP1-2α/TAZ heterodimerization is crucial for enhancing gene regulatory capacity, as well as for its role in LLPS formation. Since LLPS-mediated nuclear condensate formation is closely associated with transcriptional regulation via super-enhancer activation (22), we hypothesized that the YAP1-2α/TAZ/TEAD complex stimulates potential super-enhancer elements. To test this possibility, we analyzed the identified super-enhancer elements upstream of the *CCN1* and *CCN2* genes using public super-enhancer database SEdb3.0 (http://www.licpathway.net/sedb). Super-enhancer elements in serous ovarian cancer cells (39) and triple-negative

breast cancer cells (40) were identified from active enhancer maker H3K27ac ChIP-seq datasets using ROSE (Rank Ordering of Super-Enhancers) algorithm. Consistent with aforementioned results, identified super-enhancer elements were present upstream of the *CCN1* gene but not *CCN2* (Fig. 4*D*, Fig. S4*E*). Additionally, these elements contain TEAD-binding sites, which led us to focus on these regions as potential super-enhancers that could be activated by the YAP1-2α/TAZ/TEAD-LLPS. Using YAP1-2-reconstituted cells described in Figure 1*C*, we tested the enrichment of BRD4, a super-enhancer marker (22, 36), along with YAP1, TAZ, and TEAD at the predicted TEAD-positive enhancer region upstream of *CCN1*. In cells ectopically expressing YAP1-2α, the levels of BRD4, YAP1, TAZ, and TEAD were significantly enriched in the upstream regions of *CCN1* [-0.3 kb from the transcription start site (TSS), -0.85 kb from TSS] compared to cells ectopically expressing YAP1-2γ (Fig. 4*E*). Furthermore, ChIP-re-chip analysis corroborated that the YAP1-2α/TAZ complex was bound to these regions in a TEAD-dependent manner (Fig. 4, *F*-*G*), indicating that the YAP1-2α/TAZ/TEAD complex was specifically bound to the super-enhancer elements along with BRD4. Consistently, increased *CCN1* expression by YAP1-2α was suppressed using JQ1 (Fig. 4*H*, Fig. S4*F*), a selective inhibitor of BRD4-regulated super-enhancers (41). These results provided strong evidence that the YAP1-2α/TAZ/TEAD complex specifically activated the super-enhancer.

High YAP1-2α expression associates with the EMT signature in HGSOC

To investigate differences in gene expression profiles in same cancer species expressing differential levels of *YAP1* splice variants, we analyzed RNA-seq data from high-grade serous ovarian cancer (HGSOC) in the TCGA public database (42-44). Information on *YAP1* mRNA splicing variant PSI (percent spliced in index) data was obtained from TCGA SpliceSeq (45) Expression of *YAP1* isoforms were defined as "*YAP1-*$\alpha^{dominant}$" [PSI (*YAP1-exon 6*) < median, PSI (*YAP1-exon 5.2*) < median], "*YAP1-*$\beta^{dominant}$" [PSI (*YAP1-exon 6*) < median, PSI (*YAP1-exon 5.2*) > median], "*YAP1-*$\gamma^{dominant}$" [PSI (*YAP1-exon 6*) > median, PSI (*YAP1-exon 5.2*) < median], or "*YAP1-*$\delta^{dominant}$" [PSI (*YAP1-exon 6*) > median, PSI (*YAP1-exon 5.2*) > median]. With this HGSOC subgrouping, 754 genes were significantly upregulated in the *YAP1-*$\alpha^{dominant}$ group compared to the *YAP1-*$\gamma^{dominant}$ group (Fig. 5*A*). On the other hand, 146 genes were upregulated in the *YAP1-*$\gamma^{dominant}$ group, indicating that *YAP1-*$\alpha^{dominant}$ group is transcriptionally more active than the *YAP1-*$\gamma^{dominant}$ group. The finding is totally consistent with the fact that super-enhancer activation is characterized by the activation of a greater number of genes. Hallmark gene set analysis revealed that the elevated 754 genes were substantially associated with EMT and angiogenesis (Fig. 5*B*). In particular, EMT-associated genes (*SNAI2*, *SPARC*) (8, 46) and *ALDH1A3*, a marker of cancer stem-like cells (47), were significantly elevated in the *YAP1-*$\alpha^{dominant}$ group compared to other groups without an increase in *YAP1* and *TAZ*

mRNA levels (Fig. S5*A*). In this regard, previous reports have shown that YAP1 regulates the gene expression of *SNAI2* (8), *ALDH1A* (48), and *SPARC* (49). Furthermore, these genes have been shown to enhance EMT, acquisition of cancer stem cell-like properties, drug resistance, and invasion in cancer cells, including serous ovarian cancer (50-52). Indeed, YAP1-2α-expressing serous ovarian cancer cells exhibited significantly increased gene expression of *SPARC*, *ALDH1A3*, and *SNAI2* compared to YAP1-2γ-expressing cells (Fig. 5*C*, Fig. S5*B*). Notably, treatment with the BRD4 inhibitor JQ1 inhibited LLPS-mediated YAP1-2α puncta formation and suppressed the increased expression of *SPARC* and *ALDH1A3* by YAP1-2α (Fig. 5, *C*-*D*), suggesting that YAP1-2α potentially activates these genes by stimulating the YAP1-2α/TAZ/TEAD super-enhancers. Therefore, we further investigated the TEAD-positive super-enhancer elements upstream of the *ALDH1A3* and *SPARC*, revealing the presence of potential super-enhancer elements (Fig. S5*C*). To verify whether YAP1/TAZ/TEAD/BRD4 enriches at the potential super-enhancer elements in an YAP1 isoform dependent-manner, especially between YAP1-2α (which forms efficient LLPS) and YAP1-2γ (which does not form efficient LLPS), we used YAP1-reconstituted cells to evaluate the enrichment of BRD4, YAP1, TAZ, and TEAD in potential TEAD-positive super-enhancer elements upstream of the *SPARC* and *ALDH1A3*. Cells expressing only YAP1-2α exhibited significant enrichment of super-enhancer marker (BRD4), TAZ, and TEAD, along with YAP1, in the predicted TEAD-

positive super-enhancer elements upstream of the *SPARC* (-0.67 kb, -3.2 kb from TSS) and *ALDH1A3* (-0.52 kb from TSS). In contrast, this enrichment was not observed in cells ectopically expressing YAP1-2γ (Fig. 5*E*, Fig. S5*D*). The elevated expression levels of *SPARC* and *ALDH1A3* in UWB1.289 cells with ectopic overexpression of YAP1-2α were suppressed by *TAZ* knockout (Fig. 5*F*). Of note, when only TAZ was overexpressed, the expression of these genes decreased rather than increased, even under conditions that enhance the expression of typical TEAD target genes. (Fig. S5, *E-F*). These findings suggested that, in the LLPS formation initiated by YAP1-2α and TAZ heterodimerization, the amount of the YAP1-2α isoform serves as a rate-limiting factor, which specifically stimulates YAP1-2α/TAZ/TEAD super-enhancers to activate genes associated with EMT and cancer stem-like properties.

YAP1-2α enhances cancer hallmarks and correlates with malignant grade of HGSOC

The aforementioned results indicated that increased YAP1-2α activates EMT through transcriptional regulation. EMT potentiates cancer stem-like properties and is characterized by elevated robustness and stiffness of cancer phenotypes, exemplified by "Hallmarks of cancer", contributing to increased invasion, metastasis, resistance to oxidative stress including ferroptosis, and resistance to various cancer therapies (53, 54). Since malignant progression of cancer cells is correlated with enhanced 3D

spheroid culture (55), we compared the sphere-forming capacity of YAP1-2α-overexpressing UWB1.289 cells with that of YAP1-2γ-overexpressing UWB1.289 cells. In 2D culture, both YAP1-2α- and YAP1-2γ-overexpressing cells slightly enhanced cell proliferation compared to control cells. However, there was no substantial difference in proliferation between cells overexpressing YAP1-2α and YAP1-2γ. (Fig. 6*A*). In striking contrast, in 3D culture, the anchorage-independent growth of YAP1-2α-overexpressing cells was much greater than that of YAP1-2γ-expressing cells (Fig. 6*B*). The enhanced sphere-forming capacity of cells overexpressing YAP1-2α was suppressed by treatment with K-975 or JQ1 (Fig. 6*C*). YAP1-2α-overexpressing cells also showed more aggressive characters, including elevated chemotaxis (Fig. 6*D*, left), increased invasion into the extracellular matrix (Fig. 6*D*, right), and enhanced resistance to oxidative stress such as ferroptosis (Fig. 6*E*) in a TEAD/BRD4 dependent manner. Resistance of cancer cells to ferroptosis is associated with cellular resistance to anti-cancer drugs, including VEGF inhibitors, EGFR inhibitors, and genotoxic reagents (56). Consistently, YAP1-2α-overexpressing cells exhibited elevated resistance to various anticancer agents, including molecular targeted drugs (Trametinib) and genotoxic drugs (Cisplatin, Olaparib) (Fig. S6*A*). Notably, aforementioned phenotypes were suppressed by BRD4 inhibition, suggesting that at least the activation of super-enhancers by YAP1-2α contributes to the acquisition of malignant properties in cancer cells.

Using clinical cancer specimens, we also investigated the association between YAP1-2α expression and malignant progression. To evaluate the levels of YAP1-2α expression in human cancer specimens, a BaseScope probe specifically recognizing *YAP1-2α* mRNA was designed. The specificity of the probe was confirmed using *YAP1*-KO UWB1.289 cells that ectopically expressed YAP1-2 isoforms, respectively (Fig. S6*B*). The results of the experiment revealed that HGSOC tissues with greater YAP1-2α expression are associated with more advanced clinical stages (Fig. 6*F*, Fig. S6*C*). Additionally, an anti-YAP1 immunostaining of the cancer specimens showed that nuclear YAP1 condensates are observed in more advanced HGSOC cases exhibiting higher *YAP1-2α* expression (*YAP1-2α* staining score: 3+) (Fig. 6, *G-H*). Such condensates were hardly observed in HGSOC cases with low *YAP1-2α* expression (*YAP1-2α* staining score: 0) (Fig. S6, *D-E*). These findings suggested that YAP1-2α, a specific YAP1 isoform, enhances the robustness and resilience of cancer cells by altering transcriptional networks through LLPS formation, thereby promoting more malignant phenotypes and accelerating cancer progression.

Discussion

This study demonstrated that YAP1-2α, a specific YAP1 isoform, induces LLPS-mediated nuclear biomolecular condensates that activate TEAD-positive super-enhancers, inducing EMT-related genes that strengthen the malignant phenotype of cancer cells. In fact, elevated levels of YAP1-2α expression correlate with poor prognosis in HGSOC. YAP1-2α heterodimerizes with TAZ via the leucine zipper without influencing YAP1-2α/TEAD and TAZ/TEAD complex formation. The YAP1-2α/TAZ heterodimerization then induces LLPS that generates nuclear condensates by provoking multivalent interactions between the three WW domains in the YAP1-2α/TAZ heterodimer and the PPxY/LPxY WW domain-binding motifs present in multiple numbers in BRD4, which in turn activate YAP1-2α/TAZ/TEAD-specific super-enhancers. YAP1-1α can also heterodimerize with TAZ through the leucine zipper. However, YAP1-1α hardly induces puncta formation, presumably because of its single WW domain, which cannot mediate multivalent protein-protein interactions underlying LLPS induction. Independent of YAP1, TAZ promotes LLPS-mediated puncta formation via leucine zipper-mediated TAZ/TAZ homodimerization. In contrast to TAZ, YAP1-1α and YAP1-2α cannot homodimerize or heterodimerize, owing to the structural incompatibilities between identical leucine zipper sequences (19, 32, 57). TAZ is, therefore, capable of forming a minimum of two distinct super-enhancers, one involving the YAP1-2α/TAZ heterodimer and the other involving the

TAZ/TAZ homodimer, each of which may regulate different sets of target genes.

YAP1 and TAZ regulate numerous genes, including those involved in cell proliferation, cell-cell contact, cell polarity, cellular stress, cell metabolism, and cell cycle (7-13). Despite their redundant roles in gene regulation, as their primary partner transcription factors are TEADs (TEAD1-4), most studies have suggested that the YAP1/TEAD and TAZ/TEAD transcriptional complexes function independently (57, 58). Among the eight YAP1 isoforms present in human cells by differential splicing of *YAP1* pre-mRNA (14, 15), YAP1-2γ and YAP1-2δ, which lack a functional leucine zipper, are abundantly expressed in normal and cancer cells. Consequently, our understanding of the YAP1/TAZ heterodimer was very limited until the discovery that the minor YAP1 isoforms, YAP1-1α and YAP1-2α, can bind TAZ via leucine zippers (19). The present study further revealed that YAP1-2α/TAZ heterodimerization specifically activates EMT-related genes, contributing to elevated malignant traits in cancer cells. Indeed, a comprehensive analysis of YAP1 splicing isoforms reported that YAP1-2α also shows distinct transcriptional regulation compared to other isoforms and is responsible for higher transcriptional activity of typical TEAD target genes (16). The study strongly supports our conclusion that YAP1-2α promotes nuclear puncta formation and enhances transcriptional activity distinct from other isoforms. Additionally, NIH3T3 cells expressing YAP1-2α was shown to exhibit

higher tumorigenicity *in vivo* compared to NIH3T3 cells expressing YAP1-2γ (19). Therefore, increased YAP1-2α expression plays a crucial role in the elevated *in vivo* tumorigenesis.

Several studies have reported findings regarding YAP1-containing LLPS. IFN-γ induced by sustained treatment with anti-PD-1 immunotherapy promoted formation of YAP1 LLPS in a YAP1 leucine zipper-dependent manner, which induces resistance to the treatment via elevation of key immunosuppressive target gene expression (59). Hyperosmotic stress, which promotes YAP1 LLPS, including TEAD and TAZ, alters transcriptional capacity by activating super-enhancers (60). In the present study, we discovered that YAP1-2α, a specific YAP1 splicing isoform, is essential for the efficient formation of YAP1 LLPS. Since only YAP1-1α and YAP1-2α possess a functional leucine zipper and bind to TAZ, the splicing switch of *YAP1* pre-mRNA may play a pivotal role in YAP1-LLPS formation. Although the regulatory mechanisms of *YAP1* alternative splicing remain largely unclear, it has been reported that the neonatal alternative splicing program is rewired in damaged regenerating hepatocytes to activate the Hippo-YAP1 signaling pathway (61). During this process, the YAP1 splicing switch is induced, leading to increased expression of YAP1-2α, implying that changes in the microenvironment associated with chronic tissue damage caused by inflammation and other factors may rewire splicing mechanisms and induce splicing abnormalities in genes involved in cancer progression, including YAP1.

YAP1 activates cytokines and chemokines, thereby promoting the

polarization and recruitment of myeloid-derived suppressor cells (MDSCs) and tumor-associated macrophages (TAMs), which subsequently inactivate T cells (62, 63). Indeed, TCGA HGSOC cohort indicated that *YAP1-α*^{dominant} cancers exhibit elevated inflammatory response signaling. Also, it has been reported that interferon-γ induces leucine zipper motif-dependent phase separation of YAP1, which activates target genes involved in immunosuppression (59). This activation may be mediated by YAP1/TAZ/TEAD super-enhancers, thereby facilitating immune evasion by cancer cells. YAP1-2α/TAZ/TEAD LLPS-mediated gene regulation may therefore augment cell-intrinsic robustness while creating cell-extrinsic conditions that foster cancer cells, establishing a "cold" immune environment that contributes to the malignant progression of cancer.

The present study elucidated an unanticipated molecular connection between alternative mRNA splicing (splice-switching), liquid-liquid phase separation (LLPS), and gene regulations, which significantly alters cancer cell characteristics without genetic mutations. Recent studies have indicated an intimate correlation between aberrant alternative splicing and cancer (2). The findings of this study provide valuable insights into the mechanisms by which splicing abnormalities contribute to cancer progression. Activating YAP1-2α/TAZ/TEAD LLPS confers a more aggressive and malignant phenotype. In turn, the finding indicates selective inhibition of differential splicing that generates YAP1-2α mRNA or specific disruption of YAP1-2α/TAZ/TEAD-induced LLPS impedes

cancer progression.

Experimental procedures

Cell Lines

UWB1.289 cells (ATCC, CRL-2945) were cultured in 1:1 mixed medium supplemented with 3% FBS (Gibco), a 1:1 mixture of mammary epithelial cell growth medium (MEGM) (Lonza, CC-3150) without GA-1000 (gentamicin-amphotericin B mixture) and RPMI-1640 (Wako, 189-02025) supplemented with 10 mM HEPES and 1 mM sodium pyruvate. MDA-MB-436 (ATCC, HTB-130) cells were cultured in RPMI-1640 supplemented with 10% FBS (Gibco), 10 mM HEPES, and 1 mM sodium pyruvate. Lenti-X 293T cells (Clontech Laboratories, 632180) were cultured in D-MEM (Wako, 044-29765) supplemented with 10% FBS (Gibco) and 1 mM sodium pyruvate. Cells were incubated at 37 °C in 5% CO_2.

To generate gene knockout (KO) cell lines, cells were transfected with pX330-sgYAP1 or pX330-sgTAZ vector and a blasticidin S or puromycin resistance gene. After transfection, the cells were selected using blasticidin S (10 μg/ml), or puromycin (1 μg/ml) and cloned by limiting dilution.

Three-Dimensional Overlay Culture

UWB1.289 cells were suspended in 1:1 mixed medium containing 2% Matrigel (CORNING, #356231) (termed assay medium) and seeded onto Matrigel in 8-well chamber slides at 4×10^3 cells/well. Eight days after seeding, the spheroids were treated with 100 nM JQ1 (MedChemExpress, HY-13030), 1 μM K-975 (MedChemExpress, HY-138565), or DMSO as a mock control for 6 days. During cultivation, the assay medium with or without the indicated reagent was replaced every two days. After treatment with the appropriate reagents, spheroids were fixed with 2% paraformaldehyde for 20 min and collected using a cell-recovery solution (CORNING, 354253). The fixed spheroids were permeabilized with 0.5% TritonX-100 in PBS for 20 min at room temperature and subjected to immunostaining analysis. The Ferret diameters of spheroids were analyzed

by measuring images captured 14 days after seeding using the ImageJ software.

Expression Vectors

Base substitution and deletion mutants were generated using a KOD-plus-Mutagenesis kit according to the manufacturer's instructions (TOYOBO, SMK-101). Nucleotide sequences of all constructed vectors were confirmed by Sanger sequencing. See supporting information for RNAi and sgRNA target sequences.

Preparation of Lentivirus and Infections

The lentivirus was produced according to our previous protocol (64).

Live Cell Imaging

Cells transfected with mVenus-fused YAP1 isoforms were subjected to analysis to confirm the liquid-like properties (fusion event of puncta, disruption of puncta formation by treatment with Hex and FRAP). To detect the fusion event of the YAP1-2α puncta, time-lapse fluorescence images of cells transfected with mVenus-fused YAP1-2α were obtained for 120 s using a FLUOVIEW FV1200 confocal microscope (Olympus). To observe the disruption of YAP1-2α puncta formation by Hex treatment, transfected cells were treated with 1% Hex for 20 min. Twenty minutes after Hex treatment, the cells were washed and incubated for another 4 h. Fluorescence signals were detected at the indicated time points.

Fluorescence Recovery After Photobleaching (FRAP)

The mVenus-fused YAP1-2α nuclear puncta specified by the ROI were photobleached by laser irradiation. After photobleaching, time-lapse fluorescence images of the YAP1-2α puncta were obtained for 120 sec. Unbleached puncta were used as controls. The images were acquired at 3.2 second intervals using a 40x objective lens. The fluorescence intensities

of puncta obtained from a series of time-lapse images were analyzed using FLUOVIEW FV1200 software.

Immunofluorescence Staining

Cells were fixed with 2% or 4% paraformaldehyde in PBS for 15 min at room temperature or 37°C, permeabilized with 0.25% TritonX-100 in PBS for 10 min at room temperature, and blocked in blocking solution (5% BSA, 0.1% Tween20, 0.05% NaN3 in PBS) for 60 min at room temperature. For spheroid staining, fixed and collected spheroids were permeabilized with 0.5% TritonX-100 in PBS for 20 min at room temperature. Blocked cells/spheroids were incubated with primary antibodies against YAP1 (CST, 12395, 1:500, CST, 14074, 1:500), HA-tag (CST, 2367, 1:500 or CST, 3724, 1:500), TAZ (CST, 83669, 1:500), pan-TEAD (CST, 13295, 1:500), Flag-tag (SIGMA, F3165, 1:1000), BRD4 (CST, 13440, 1:500), or ki67 (Thermo Fisher Scientific, 14-5698-80, 1:500). After the antigen-antibody reaction, Alexa Fluor-conjugated secondary antibodies (1:1000) and/or Alexa Fluor-conjugated phalloidin (Invitrogen) were used. Nuclei were stained with DAPI (wako, 043-18804, 1:1000) solution.

Proximity Ligation Assay

PLA was performed using a Duolink *In situ* PLA kit (SIGMA, Duo92007, Duo92002, Duo92004) according to the manufacturer's instructions. For more details on PLA analysis, see our published protocol (64).

Immunohistochemistry

The human ovarian cancer tissue arrays (OV0071a, OV1004A, US Biomax) were deparaffinised and rehydrated. Antigen retrieval was performed by boiling for 15 minutes in 1x Target Retrieval (ACD). To block endogenous peroxidase activity, the tissue array was incubated with 3% hydrogen peroxide in double-distilled water for 10 min at room temperature. The array was then incubated overnight at 4 °C with a primary antibody against YAP1 (CST, 14074, 1:400). After the antigen-

antibody reaction, the array was incubated for 60 min at room temperature with Alexa Fluor-conjugated secondary antibodies (1:1000). After the secondary antibody reaction, the nuclei were stained with DAPI solution (1:1000) for 20 min at room temperature. Fluorescence images were obtained using FLUOVIEW FV1200 confocal microscope. H&E staining was performed using the Hematoxylin and Eosin Stain kit (ScyTek Laboratories).

In Situ Hybridization (BaseScope)

Deparaffinized and rehydrated tissue arrays were subjected to *in situ* hybridization (BaseScope). BaseScope was performed using the BaseScope Detection Reagent Kit v2-RED (ACD) according to the manufacturer's instructions. The human YAP1-1/2α-isoform-specific probe (BA-Hs-YAP1-tv3-E5E6) was designed using an ACD. The expression levels of *YAP1-2α* mRNA were determined by measuring the *YAP1-2α* mRNA BaseScope signals using the ImageJ software. *YAP1-2α* mRNA expression was scored as 0: no staining or less than 1 dot to every 20 cells; 1+: 1 dot/cell; 2+: 2-3 dots/cell, no or very few dot clusters; 3+: 4-10 dots/cell, less than 10% positive cells have dot clusters; 4+: >10 dots/cell, more than 10% positive cells have dot clusters. Staining scores were set according to the scoring guidelines of BaseScope.

Induction of Artificial Heterodimer Complexes

To induce heterodimerization of YAP1-2α(LZM)/TAZ(LZM) or YAP1-2γ/TAZ(LZM), we constructed DmrC-mSECFP-fused YAP1-2α(LZM) or DmrC-mSECFP-fused YAP1-2γ and DmrA-mVenus-fused TAZ(LZM), and transfected into UWB1.289 cells. The transfected cells were treated with A/C heterodimerizer (Clontech, Z5057N) according to the manufacturer's instructions and subjected to an immunoprecipitation analysis, a live cell imaging analysis, or a qPCR analysis.

Immunoprecipitation and Immunoblotting

The cells were washed in ice-cold PBS and lysed in lysis buffer (100 mM NaCl, 50 mM Tris-HCl pH 7.5, 5 mM EDTA, 2 mM Na_3VO_4, 10 mM NaF, 10 mM β-glycerophosphate, 2 mM PMSF, 10 μg/ml leupeptin, 10 μg/ml trypsin inhibitor, 10 μg/ml aprotinin, and 0.4% NP-40). Cell lysates were incubated with protein G-beads after incubation with anti-TAZ, anti-HA, anti-Flag antibody, or isotype control IgG. The beads were washed five times with lysis buffer, and the immunoprecipitates were eluted using SDS sample buffer. The immunoprecipitates and total cell lysates were subjected to SDS-PAGE, followed by immunoblotting. The images were captured using the LAS-4000 imager (FUJIFILM). To compare protein expression levels, protein band intensities obtained from three biological replicate experiments were collected and quantitatively analyzed using LAS-4000 imager (FUJIFILM).

Chromatin immunoprecipitation

To evaluate interaction between genome DNA and target proteins, DNA samples were prepared using the CUT & RUN and the ChIP-re-chip. CUT & RUN was performed using CUT & RUN Assay Kit (CST) according to the manufacturer's instructions, employing anti-BRD4 (CST, 13440, 1:50), anti-HA (CST, 3724, 1:50), anti-TAZ (CST, 83669, 1:50), or anti-panTEAD (CST, 13295, 1:50) antibody. Rabbit IgG (CST, 66362, 1: 20) was used as the isotype control. For ChIP-re-chip, *YAP1*-KO UWB1.289 cells were transfected with 6xHis-tagged YAP1-2α and treated with K-975 or DMSO. Twenty-four hours after K-975 treatment, a cross-linking reaction with formaldehyde (CST, 12606) was performed, followed by chromatin isolation and sonication. Cross-linked chromatin was pulled down using Ni Sepharose excel (Cytiva) and eluted with 500 mM imidazole. The imidazole was replaced with a lysis buffer by centrifugal ultrafiltration (Millipore, UFC903024), and immunoprecipitation was performed using anti-TAZ antibody (CST, 83669) or rabbit IgG (CST,

66362) as an isotype control. Chromatin bound to YAP1-2α/TAZ complex was reversed and the DNA fragments were purified using spin columns (CST, 14209). Purified DNA samples were subjected to PCR or qPCR analysis.

Quantitative PCR (qPCR)

Total RNA was extracted from cells using TRIzol reagent (Invitrogen) and reverse-transcribed using the High-Capacity cDNA Reverse Transcription Kit (Thermo Fisher Scientific, 4368814). Relative mRNA expression was analyzed using the QuantStudio 3 Real-Time PCR System (Thermo Fisher Scientific) with SYBR *Premix Ex Taq* Tli RNaseH Plus (TaKaRa). *18S* rRNA was used as an internal control. The data were analyzed using the comparative CT (ΔΔCT) method. For ChIP-qPCR analysis, purified DNA fragments prepared by CUT & RUN and ChIP-re-chip were analyzed using the QuantStudio 3 Real-Time PCR System with KOD-SYBR qPCR Mix (TOYOBO). See supporting information for primer sequences.

Luciferase Reporter Assay

A luciferase reporter assay was performed using a dual luciferase reporter assay kit (Promega). See our previous work for details (64). To examine the effect of YAP1-2α mutants on TEAD activity, *YAP1*-KO UWB1.289 cells were transfected with the TEAD reporter plasmid together with the indicated mVenus-fused YAP1-2α mutant expression vector (wild-type, LZM, S94A, LZM|S94A) using Lipofectamine 2000 reagent (Invitrogen), and 48 h after transfection, cells were collected using passive lysis buffer (Promega). Luminescence was detected using a Centro XS^3 LB960 (BERTHOLD). The relative luciferase activities were calculated as fold changes relative to the values of the control samples. To confirm the protein expression levels of the mVenus-fused YAP1-2α mutants, the remaining cell lysates were subjected to immunoblotting.

Cell Viability Assay

Sensitivity to anti-cancer agents and 2D cell proliferation was measured by MTS assay using CellTiter 96 AQueous One Solution Cell Proliferation Assay (Promega, G3580) according to the manufacturer's instructions. To examine drug sensitivity, 1,000 cells were seeded into each well of 96-well plates and treated with stepwise concentrations of anticancer agents (Cisplatin, Sorafenib, Trametinib) for 72 h. To examine sensitivity to Olaparib, 500 cells were seeded into each well of 96-well plates and treated with a stepwise concentration of Olaparib for 6 days. After treatment with anti-cancer agents, the cells were incubated with the MTS assay reagent at 37 °C in 5% CO_2. After 60-90 min of incubation, the absorbance at 490 nm was measured using Multiskan FC (Thermo Fisher Scientific). The relative cell viability was calculated using mock-treated cells.

Three-dimensional Cell Viability Assay

To examine anchorage-independent growth, cells were seeded at 500 cells per well into an Ultra-Low Attachment 96-well plate (CORNING) and cultured for 12 days. During cultivation, the medium was replaced every 2 days. Appropriately cultured spheroids were lysed in CellTiter-Glo 3D Cell Viability Assay Reagent (Promega, G9683). The 200 μl cell lysate obtained from each well was immediately transferred into a white 96-well plate (Greiner) and luminescence was measured using Centro XS^3 LB960. To ensure linearity of the luminescence signal in these assays, dilution operations were performed as appropriate.

Ferroptosis Assay

Cells treated with 100 nM JQ1, 1 μM K-975, or DMSO as a mock control for 3 days were seeded into a 96-well plate (Greiner) and further treated with chlorido [N, N'-Disalicylidene-1,2-Phenylenediamine] Iron (III) (Cayman Chemical Company, 28788) or DMSO as a mock control for 48

h. Cultured cells were lysed in CellTiter-Glo 3D Cell Viability Assay reagents (Promega). Cell viability was determined by detecting luminescence using a Centro XS3 LB960.

Migration and Invasion Assay

Cells treated with 100 nM JQ1, 1 μM K-975, or DMSO as a mock control for 3 days were seeded into Transwell (Costar: 3464) inserted into 24-well plates (Coster: 3526). Transwell coated with type-I-A collagen gel (Wako), prepared according to the manufacturer's protocols, was used to examine the ability of the cells to infiltrate the extracellular matrix (invasion assay). The cells were further cultured in medium containing 0.1% FBS for 48 h (chemotaxis assay) or 2 weeks (invasion assay). The bottom wells were filled with medium containing 10% FBS. After incubation for the appropriate time, cells that had migrated or infiltrated into the lower wells were lysed in CellTiter-Glo 3D Cell Viability Assay regents. The cell number was determined by detecting luminescence using Centro XS3 LB960.

Prediction of Molecular Complex Structure

The complex structure of WW1 or WW2 domain of YAP1-2α with the BRD4 LPxY or PPxY motif was predicted using AlphaFold2 multimer via the Colabfold v1.5.5 web server (https://colab.research.google.com/github/sokrypton/ColabFold/blob/main/AlphaFold2.ipynb). The buried surface area of the LPxY or PPxY motifs in the complex was estimated using the PDBePISA web server (https://www.ebi.ac.uk/pdbe/pisa/). Structural graphics were generated using PyMOL v2.5.0.

Analysis of HGSOC RNA-seq Data

PSI [percent spliced in index: the ratio of normalized read counts indicating inclusion of a transcript element over the total normalized reads for that event (both inclusion and exclusion reads)] data for the *YAP1*

mRNA splicing variants containing γ-segment (referred to as *YAP1-E6*) and *YAP1* mRNA splicing variants containing β-segment (referred to as *YAP1-E5.2*) were downloaded directly from the TCGA SpliceSeq (https://bioinformatics.mdan derson.org/TCGASpliceSeq/singlegene.jsp) (45). HGSOC RNA-seq data was downloaded directly from the cBioportal for Cancer Genomics (https://www.cbioportal.org/) (42-44). For subgrouping the TCGA cohorts, expression of *YAP1* isoforms were defined as "*YAP1-*$\alpha^{dominant}$" [PSI (*YAP1-exon 6*) < median, PSI (*YAP1-exon 5.2*) < median], "*YAP1-*$\beta^{dominant}$" [PSI (*YAP1-exon 6*) < median, PSI (*YAP1-exon 5.2*) > median], "*YAP1-*$\gamma^{dominant}$" [PSI (*YAP1-exon 6*) > median, PSI (*YAP1-exon 5.2*) < median], or "*YAP1-*$\delta^{dominant}$" [PSI (*YAP1-exon 6*) > median, PSI (*YAP1-exon 5.2*) > median]. HGSOC patients (n = 425) were divided into the "*YAP1-*$\alpha^{dominant}$" (n = 131), "*YAP1-*$\beta^{dominant}$" (n = 83), "*YAP1-*$\gamma^{dominant}$" (n = 78), and "*YAP1-*$\delta^{dominant}$" (n = 133). TPM count for "*YAP1-*$\alpha^{dominant}$" and "*YAP1-*$\gamma^{dominant}$" were analyzed using iDEP v2.4.0 web tool (https://bioinformatics.sdstate.edu/idep/) (65) to perform DEG analysis. Genes whose expression increased in "*YAP1-*$\alpha^{dominant}$" vs. "*YAP1-*$\gamma^{dominant}$" (FDR < 0.1, FC >1.5) were further subjected to gene enrichment analysis (Hallmark MSigDB) using the gene-set enrichment tool ShinyGO (https://bioinformatics.sdstate.edu/go/) (66).

Prediction of SE elements

Identified super-enhancer elements in serous ovarian cancer cells (GSM3328052: PEO1) (39) and triple-negative breast cancer cells (GSM6132824: MDA-MB-436) (40) were downloaded from SEdb3.0 (http://www.licpathway.net/sedb). TEAD1 and TEAD4-binding motif elements were downloaded from JASPR (https://jaspar.elixir.no/) (67). The downloaded data were visualized using IGV (https://igv.org/app/).

Statistical analysis

The specific statistical methods used are indicated in the figure legends,

and were calculated using Microsoft Excel and PRISM GraphPad software. Unpaired T-tests (Student's T-test and Welch's T-test) and U-tests were performed to compare the two groups. Details of the analysis are provided in the respective methods. All experiments presented in the manuscript were repeated in three technical or biological replicates.

Data availability

All the other data supporting the findings of this study are available within the article and its supplementary information files.

This study did not generate the original code.

Supporting information

Supporting information includes 6 figures and 2 tables, which can be found with this article online.

Author contributions

T.O., (for all experiments), T.H. (for Prediction of Molecular Complex Structure) and Y. Y. (for qPCR analysis and immunoblotting) performed the experiments. T.O. analyzed data. T.O. designed the study. T.O. and M.H. wrote the paper. T.H. reviewed the paper. M.H. supervised this work.

Funding and additional information

This work was supported by a JSPS Grant-in-Aid for Scientific Research from the Japan Society for the Promotion of Science Grant numbers 21H04804 (M.H.) 24H00618 (M.H), and JP21K15526 (T.O.), P-PROMOTE from AMED Grant Number JP23ama221219h0001 (M.H.), and Microbial Chemistry Research and Development Fund Grant Number 23A02 (T.O.).

Further information and requests should be addressed to the lead contact, Masanori Hatakeyama (mhata@m.u-tokyo.ac.jp).

Conflict of interest

The authors declare no competing interests.

References

1. Oltean, S., and Bates, D.O. (2014) Hallmarks of alternative splicing in cancer. *Oncogene*. **33**, 5311-8
2. Bradley, R.K., and Anczuków, O. (2023) RNA splicing dysregulation and the hallmarks of cancer. *Nat Rev Cancer*. **23**, 135-155
3. Peng, Q., Zhou, Y., Oyang, L., Wu, N., Tang, Y., Su, M., Luo, X., Wang, Y., Sheng, X., Ma, J., and Liao, Q. (2022) Impacts and mechanisms of alternative mRNA splicing in cancer metabolism, immune response, and therapeutics. *Mol Ther*. **30**, 1018-1035
4. Zhao, B., Ye, X., Yu, J., Li, L., Li, W., Li, S., Yu, J., Lin, J.D., Wang, C.Y., Chinnaiyan, A.M., et al. (2008) TEAD mediates YAP-dependent gene induction and growth control. *Genes Dev*. **22**, 1962-1971
5. Zhang, H., Liu, C.Y., Zha, Z.Y., Zhao, B., Yao, J., Zhao, S., Xiong, Y., Lei, Q.Y., and Guan, K.L. (2009) TEAD transcription factors mediate the function of TAZ in cell growth and epithelial-mesenchymal transition. *J. Biol. Chem*. **284**, 13355-13362
6. Zanconato, F., Battilana, G., Forcato, M., Filippi, L., Azzolin, L., Manfrin, A., Quaranta, E., Di, Biagio. D., Sigismondo, G., Guzzardo, V., et al. (2018) Transcriptional addiction in cancer cells is mediated by YAP/TAZ through BRD4. *Nat Med*. **24**, 1599-1610
7. Zheng, Y., and Pan, D. (2019) The Hippo signaling pathway in development and disease. *Dev. Cell*. **50**, 264-282
8. Thrash, H.L., and Pendergast, A.M. (2023) Multi-functional regulation by YAP/TAZ signaling networks in tumor progression and metastasis. *Cancers*. **15**, 4701
9. Kim, M.H., and Kim, J. (2017) Role of YAP/TAZ transcriptional regulators in resistance to anti-cancer therapies. *Cell. Mol. Life Sci*. **74**, 1457-1474
10. Shao, D.D., Xue, W., Krall, E.B., Bhutkar, A., Piccioni, F., Wang, X., Schinzel, A.C., Sood, S., Rosenbluh, J., Kim, J.W., et al. (2014) KRAS and YAP1 converge to regulate EMT and tumor survival. *Cell*. **158**, 171-184

11. Lin, L., Sabnis, A.J., Chan, E., Olivas, V., Cade, L., Pazarentzos, E., Asthana, S., Neel, D., Yan, J.J., Lu, X., et al. (2015) The Hippo effector YAP promotes resistance to RAF- and MEK-targeted cancer therapies. *Nat. Genet*. **47**, 250-256
12. Zanconato, F., Forcato, M., Battilana, G., Azzolin, L., Quaranta, E., Bodega, B., Rosato, A., Bicciato, S., Cordenonsi, M., and Piccolo, S. (2015) Genome-wide association between YAP/TAZ/TEAD and AP-1 at enhancers drives oncogenic growth. *Nat. Cell Biol.* **17**, 1218-1227
13. He, L., Pratt, H., Gao, M., Wei, F., Weng, Z., and Struhl, K. (2021) YAP and TAZ are transcriptional coactivators of AP-1 proteins and STAT3 during breast cellular transformation. *Elife*. **10**, e67312
14. Gaffney, C.J., Oka, T., Mazack, V., Hilman, D., Gat, U., Muramatsu, T., Inazawa, J., Golden, A., Carey, D.J., Farooq, A., et al. (2012) Identification, basic characterization and evolutionary analysis of differentially spliced mRNA isoforms of human YAP1 gene. *Gene*. **509**, 215-222
15. Sudol, M. (2013) YAP1 oncogene and its eight isoforms. *Oncogene*. **32**, 3922
16. Vrbský, J., Vinarský, V., Perestrelo, A.R., De La Cruz, J.O., Martino, F., Pompeiano, A., Izzi, V., Hlinomaz, O., Rotrekl, V., Sudol, M., Pagliari, S., and Forte, G. (2021) Evidence for discrete modes of YAP1 signaling via mRNA splice isoforms in development and diseases. *Genomics*. **113**, 1349-1365
17. Ingham, R.J., Colwill, K., Howard, C., Dettwiler, S., Lim, C.S.H., Yu, J., Hersi, K., Raaijmakers, J., Gish, G., Mbamalu, G., et al. (2005) WW domains provide a platform for the assembly of multiprotein networks. *Mol. Cell. Biol*. **25**, 7092-7106
18. Yang, Y., Wu, M., Pan, Y., Hua, Y., He, X., Li, X., Wang, J., and Gan, X. (2024) WW domains form a folded type of nuclear localization signal to guide YAP1 nuclear import. *J Cell Biol*. **223**, e202308013
19. Ben, C., Takahashi-Kanemitsu, A., Wu, X., Knight, C.K., and Hatakeyama, M. (2020) Alternative splicing reverses the cell-intrinsic and cell-extrinsic

prooncogenic potentials of YAP1 via SHP2. *J. Biol. Chem.* **295**, 13965-13980

20. Huang, Z., Liu, Z., Chen, L., Liu, Y., Yan, G., Ni, Y., Yan, Q., He, W., Liu, J., Luo, S., and Xie, J. (2025) Liquid-liquid phase separation in cell physiology and cancer biology: recent advances and therapeutic implications. *Front Oncol.* **15**, 1540427
21. Wang, B., Zhang, L., Dai, T., Qin, Z., Lu, H., Zhang, L., and Zhou, F. (2021) Liquid-liquid phase separation in human health and diseases. *Signal Transduct Target Ther.* **6**, 290
22. Sabari, B.R., Dall'Agnese, A., Boija, A., Klein, I.A., Coffey, E.L., Shrinivas, K., Abraham, B.J., Hannett, N.M., Zamudio, A.V., Manteiga, J.C., et al. (2018) Coactivator condensation at super-enhancers links phase separation and gene control. *Science.* **361**, eaar3958
23. Whyte, W.A., Orlando, D.A., Hnisz, D., Abraham, B.J., Lin, C.Y., Kagey, M.H., Rahl, P.B., Lee, T.I., and Young, R.A. (2013) Master transcription factors and mediator establish super-enhancers at key cell identity genes. *Cell.* **153**, 309-319
24. Hnis, D., Abraham, B., Lee, T.I., Lau, A., Saint-André, V., Sigova, A.A., Hoke, H.A., and Young, R.A. (2013) Super-enhancers in the control of cell identity and disease. *Cell.* **155**, 934-947
25. Tan, M., Pan, Q., Gong, H., Zhai, X., Wan, Z., Ge, M., Gu, J., Zhang, D., Chen, X., and Xu, D. (2023) Super-enhancer-associated SNHG15 cooperating with FOSL1 contributes to bladder cancer progression through the WNT pathway. *Pharmacol. Res.* **197**, 106940
26. Luo, S., Luo, Y., Wang, Z., Yin, H., Wu, Q., Du, X., and Xie, X. (2024) Super-enhancer mediated upregulation of MYEOV suppresses ferroptosis in lung adenocarcinoma. *Cancer Lett.* **589**, 216811
27. Hu, X., Wu, J., Feng, Y., Ma, H., Zhang, E., Zhang, C., Sun, Q., Wang, T., Ge, Y., Zong, D., et al. (2023) METTL3-stabilized super enhancers-lncRNA SUCLG2-AS1 mediates the formation of a long-range chromatin loop between enhancers and promoters of SOX2 in metastasis and

radiosensitivity of nasopharyngeal carcinoma. *Clin. Transl. Med.* **13**, e1361

28. Tasdemir, N., Banito, A., Roe, J.S., Alonso-Curbelo, D., Camiolo, M., Tschaharganeh, D.F., Huang, C.H., Aksoy, O., Bolden, J.E., Chen, C.C., et al. (2016) BRD4 connects enhancer remodeling to senescence immune surveillance. *Cancer Discov.* **6**, 612-629
29. Li, G.H., Qu, Q., Qi, T.T., Teng, X.Q., Zhu, H.H., Wang, J.J., Lu, Q., and Qu, J. (2021) Super-enhancers: a new frontier for epigenetic modifiers in cancer chemoresistance. *J. Exp. Clin. Cancer Res.* **40**, 174
30. Ganser, L.R., and Myong, S. (2020) Methods to Study Phase-Separated Condensates and the Underlying Molecular Interactions. *Trends Biochem Sci.* **45**, 1004-1005
31. Kaneda, A., Seike, T., Danjo, T., Nakajima, T., Otsubo, N., Yamaguchi, D., Tsuji, Y., Hamaguchi, K., Yasunaga, M., Nishiya, Y., et al. (2020) The novel potent TEAD inhibitor, K-975, inhibits YAP1/TAZ-TEAD protein-protein interactions and exerts an anti-tumor effect on malignant pleural mesothelioma. *Am. J. Cancer Res.* **10**, 4399-4415
32. Lu, Y., Wu, T., Gutman, O., Lu, H., Zhou, Q., Henis, Y.I., and Luo, X. (2020) Phase separation of TAZ compartmentalizes the transcription machinery to promote gene expression. *Nat. Cell Biol.* **22**, 453-464
33. Guo, Q., Quan, M., Dong, J., Bai, J., Wang, J., Han, R., Wang, W., Cai, Y., et al. (2020) The WW domains dictate isoform-specific regulation of YAP1 stability and pancreatic cancer cell malignancy. *Theranostics* **10**, 4422-4436
34. Hatstat, A.K., Pupi, M.D., and McCafferty, D.G. (2021) Predicting PY motif-mediated protein-protein interactions in the Nedd4 family of ubiquitin ligases. *PLoS One* **16**, e0258315
35. Mehta, S., and Zhang, J. (2022) Liquid-liquid phase separation drives cellular function and dysfunction in cancer. *Nat. Rev. Cancer* **22**, 239-252
36. Qian, H., Zhu, M., Tan, X., Zhang, Y., Liu, X., and Yang, L. (2023) Super-enhancers and the super-enhancer reader BRD4: tumorigenic factors and therapeutic targets. *Cell Death Discov.* **9**, 470

37. Conaway, R.C., and Conaway, J.W. (2011) Function and regulation of the mediator complex. *Curr. Opin. Genet. Dev.* **21**, 225-230
38. Han, X., Yu, D., Gu, R., Jia, Y., Wang, Q., Jaganathan, A., Yang, X., Yu, M., Babault, N., Zhao, C., et al. (2020) Roles of the BRD4 short isoform in phase separation and active gene transcription. *Nat. Struct. Mol. Biol.* **27**, 333-341
39. Chung, V.Y., Tan, T.Z., Ye, J., Huang, R.L., Lai, H.C., Kappei, D., Wollmann, H., Guccione, E., and Huang, R.Y. (2019) The role of GRHL2 and epigenetic remodeling in epithelial-mesenchymal plasticity in ovarian cancer cells. *Commun Biol.* **2**, 272
40. Jovanović, B., Temko, D., Stevens, L.E., Seehawer, M., Fassl, A., Murphy, K., Anand, J., Garza, K., Gulvady, A., Qiu, X., et al. (2023) Heterogeneity and transcriptional drivers of triple-negative breast cancer. *Cell Rep.* **42**, 113564
41. Filippakopoulos, P., Qi, J., Picaud, S., Shen, Y., Smith, W.B., Fedorov, O., Morse, E.M., Keates, T., Hickman, T.T., Felletar, I., et al. (2010) Selective inhibition of BET bromodomains. *Nature* **468**, 1067-1073
42. Cerami, E., Gao, J., Dogrusoz, U., Gross, B.E., Sumer, S.O., Aksoy, B.A., Jacobsen, A., Byrne, C.J., Heuer, M.L., Larsson, E., et al. (2012) The cBio cancer genomics portal: an open platform for exploring multidimensional cancer genomics data. *Cancer Discov.* **2**, 401-404
43. Gao, J., Aksoy, B.A., Dogrusoz, U., Dresdner, G., Gross, B., Sumer, S.O., Sun, Y., Jacobsen, A., Sinha, R., Larsson, E., et al. (2013) Integrative analysis of complex cancer genomics and clinical profiles using the cBioPortal. *Sci. Signal.* **6**, pl1
44. de Bruijn, I., Kundra, R., Mastrogiacomo, B., Tran, T.N., Sikina, L., Mazor, T., Li, X., Ochoa, A., Zhao, G., Lai, B., et al. (2023) Analysis and visualization of longitudinal genomic and clinical data from the AACR project GENIE Biopharma Collaborative in cBioPortal. *Cancer Res.* **83**, 3861-3867

45. Ryan, M., Wong, W.C., Brown, R., Akbani, R., Su, X., Broom, B., Melott, J., and Weinstein, J. (2016) TCGASpliceSeq a compendium of alternative mRNA splicing in cancer. *Nucleic Acids Res*. **44**, D1018-1122
46. Fenouille, N., Tichet, M., Dufies, M., Pottier, A., Mogha, A., Soo, J.K., Rocchi, S., Mallavialle, A., Galibert, M.D., Khammari, A., et al. (2012) The epithelial-mesenchymal transition (EMT) regulatory factor SLUG (SNAI2) is a downstream target of SPARC and AKT in promoting melanoma cell invasion. *PLoS One*. **7**, e40378
47. McLean, M.E., MacLean, M.R., Cahill, H.F., Arun, R.P., Walker, O.L., Wasson, M.D., Fernando, W., Venkatesh, J., and Marcato, P. (2023) The Expanding Role of Cancer Stem Cell Marker ALDH1A3 in Cancer and Beyond. *Cancers (Basel)*. **15**, 492
48. Bauzone, M., Souidi, M., Dessein, A.F., Wisztorski, M., Vincent, A., Gimeno, J.P., Monté, D., Van Seuningen, I., Gespach, C., and Huet, G. (2021) Cross-talk between YAP and RAR-RXR Drives Expression of Stemness Genes to Promote 5-FU Resistance and Self-Renewal in Colorectal Cancer Cells. *Mol Cancer Res*. **19**, 612-622
49. Xiao, Y., Zhang, H., Ma, Q., Huang, R., Lu, J., Liang, X., Liu, X., Zhang, Z., Yu, L., Pang, J., Zhou, L., Liu, T., Wu, H., and Liang, Z. (2019) YAP1-mediated pancreatic stellate cell activation inhibits pancreatic cancer cell proliferation. *Cancer Lett*. **462**, 51-60
50. Guo, X., Tai, H., Li, X., Liu, P., Liu, J., and Yu, S. (2024) SPARC is a Novel Prognostic Biomarker for Ovarian Cancer and Associated with Immune Signatures and Drug Response. *Clin. Exp. Obstet. Gynecol*. **51**, 61
51. Chen, J., Wang, M., Xi, B., Xue, J., He, D., Zhang, J., and Zhao, Y. (2012) SPARC is a key regulator of proliferation, apoptosis and invasion in human ovarian cancer. *PLoS One*. **7**, e42413
52. Huang, J., Tang, Y., Li, Y., Wei, W., Kang, F., Tan, S., Lin, L., Lu, X., Wei, H., and Wang, N. (2024) ALDH1A3 contributes to tumorigenesis in high-grade serous ovarian cancer by epigenetic modification. *Cell Signal*. **116**, 111044

53. Dart, A. (2023) EMT in chemoresistance. *Nat. Rev. Cancer*. **23**, 349
54. Hanahan, D., and Weinberg, R.A. (2000) The hallmarks of cancer. *Cell*. **100**, 57-70
55. Zhang, C., Yang, Z., Dong, D.L., Jang, T.S., Knowles, J.C., Kim, H.W., Jin, G.Z., and Xuan, Y. (2020) 3D culture technologies of cancer stem cells: promising ex vivo tumor models. *J. Tissue Eng.* **11**, 1-17
56. Zhang, C., Liu, X., Jin, S., Chen, Y., and Guo, R. (2022) Ferroptosis in cancer therapy: a novel approach to reversing drug resistance. *Mol Cancer*. **21**, 47
57. Kaan, H.Y.K., Chan, S.W., Tan, S.K.J., Guo, F., Lim, C.J., Hong, W., and Song, H. (2017) Crystal structure of TAZ-TEAD complex reveals a distinct interaction mode from that of YAP-TEAD complex. *Sci. Rep*. **7**, 2035
58. Cunningham, R., and Hansen, C.G. (2022) The Hippo pathway in cancer: YAP/TAZ and TEAD as therapeutic targets in cancer. *Clin. Sci. (Lond)* **136**, 197-222
59. Yu, M., Peng, Z., Qin, M., Liu, Y., Wang, J., Zhang, C., Lin, J., Dong, T., Wang, L., Li, S., et al. (2021) Interferon-γ induces tumor resistance to anti-PD-1 immunotherapy by promoting YAP phase separation. *Mol. Cell* **81**, 1216-1230
60. Cai, D., Feliciano, D., Dong, P., Flores, E., Gruebele, M., Porat-Shliom, N., Sukenik, S., Liu, Z., and Lippincott-Schwartz, J. (2019) Phase separation of YAP reorganizes genome topology for long-term YAP target gene expression. *Nat Cell Biol*. **21**, 1578-1589
61. Bangru, S., Arif, W., Seimetz, J., Bhate, A., Chen, J., Rashan, E.H., Carstens, R.P., Anakk, S., and Kalsotra, A. (2018) Alternative splicing rewires Hippo signaling pathway in hepatocytes to promote liver regeneration. *Nat Struct Mol Biol*. **25**, 928-939.
62. Wang, G., Lu, X., Dey, P., Deng, P., Wu, C.C., Jiang, S., Fang, Z., Zhao, K., Konaparthi, R., Hua, S., et al. (2016) Targeting YAP-dependent MDSC infiltration impairs tumor progression. *Cancer Discov*. **6**, 80-95
63. Yang, W., Yang, S., Zhang, F., Cheng, F., Wang, X., and Rao, J. (2020) Influence of the Hippo-YAP signalling pathway on tumor associated

macrophages (TAMs) and its implications on cancer immunosuppressive microenvironment. *Ann. Transl. Med.* **8**, 399

64. Ooki, T., Murata-Kamiya, N., Takahashi-Kanemitsu, A., Wu, W., and Hatakeyama, M. (2019) High-Molecular-Weight hyaluronan is a Hippo pathway ligand directing cell density-dependent growth inhibition via PAR1b. *Dev. Cell* **49**, 590-604
65. Ge, S.X., Son, E.W., and Yao, R. (2018) iDEP: an integrated web application for differential expression and pathway analysis of RNA-Seq data. *BMC Bioinformatics.* **19**, 534
66. Ge, S.X., Jung, D., and Yao, R. (2020) ShinyGO: a graphical gene-set enrichment tool for animals and plants. *Bioinformatics.* **36**, 2628-2629
67. Rauluseviciute, I., Riudavets-Puig, R., Blanc-Mathieu, R., Castro-Mondragon, J.A., Ferenc, K., Kumar, V., Lemma, R.B., Lucas, J., Chèneby, J., Baranasic, D., et al. (2024) JASPAR 2024: 20th anniversary of the open-access database of transcription factor binding profiles. *Nucleic Acids Res.* **52**, D174-D182

Figure Legends

Figure 1. YAP1 induces LLPS in a splicing isoform dependent manner. *A-B*, *YAP1*-KO UWB1.289 cells were transfected with mVenus-fused YAP1 isoforms. The fluorescence signal of mVenus (green) and DAPI (blue) (*A*). Number of mVenus-fused YAP1 puncta per nucleus (*B*). *$p < 0.05$ (Welch's T test). n=3 (biological replicates). Error bars indicate the mean ± SD. *C*, Reconstitution of *YAP1*-KO UWB1.289 cells with a single YAP1 isoform, YAP1-2α or YAP1-2γ. YAP1 was visualized by immunofluorescence staining (green). *D-E*, Live cell imaging of *YAP1*-KO UWB1.289 cells transfected with mVenus-fused YAP1-2α. YAP1-2α fluorescence signals at the indicated time points after Hex treatment (*D*). Fusion event of YAP1-2α puncta. Yellow arrows indicate punctate fusion (*E*). *F-G*, FRAP analysis of the mVenus-fused YAP1-2α. Time-lapse images of two different *YAP1*-KO UWB1.289 cells transfected with mVenus-fused YAP1-2α are shown in Exp.1 and Exp.2. Yellow arrows indicate photobleached puncta. Images of the entire nucleus are shown in Figure S1*D*. Unbleached puncta were used as negative controls. Scale bars indicate 1 μm (*F*). Fluorescence intensities of puncta (photobleached, n=12; unbleached, n=12) were analyzed from a series of time-lapse images. τ: interval of fluorescence detection. Error bars indicate the mean ± SD (*G*). (*A*, *C-E*) Scale bars indicate 10 μm.

Figure 2. YAP1-2α/TAZ/TEAD enhancer complex initiated by YAP1-

2α/TAZ heterodimerization is required for YAP1 LLPS. *A*, Fluorescence images of mVenus-fused YAP1-2α (green) and mCherry-fused TAZ (red) (top panels). The colocalization of YAP1-2α and TAZ in the puncta was shown as white signals (bottom). *B*, Nuclear puncta formation in *YAP1*-KO UWB1.289 cells expressing the mVenus-fused YAP1-2α mutants (left). Number of YAP1 puncta in the nucleus (right). *C*, Formation of YAP1-2α puncta in the *TAZ*-KO MDA-MB-436 cells (left). Number of YAP1 puncta in the nucleus (right). *D-E*, Artificial heterodimerization between YAP1-2α(LZM) and TAZ(LZM), or YAP1-2γ and TAZ(LZM) in UWB1.289 cells using the iDimerize Induceble Heterodimer System (Clontech). Schematic view (*D*). Percentage of cells with nuclear YAP1 puncta. DmrA-mVenus is used as control (*E*). Confirmation of heterodimer formation and immunofluorescence images were shown in Figure S2*G-H*. *F*, Immunofluorescence images of mVenus-fused YAP1-2α (green) and pan-TEAD (red). The puncta indicated by white arrows are enlarged. *G*, Wild-type YAP1-2α(WT) or YAP1-2α(S94A)-transfected UWB1.289 cells were treated with K-975. Immunofluorescence images of YAP1-2α (left). Number of YAP1 puncta in the nucleus (right). *H*, UWB1.289 cells were co-transfected with mSECFP-fused YAP1-2α, mVenus-fused HA-TAZ, and Flag-TAZ and analyzed by combining FRET and PLA to detect YAP1-2α/TAZ heterodimers and TAZ/TAZ homodimers in YAP1-2α or TAZ/TAZ puncta. TAZ homodimer was visualized using PLA (red). YAP1-2α/TAZ

heterodimer was detected by SECFP/Venus FRET. White arrows indicate YAP1-2α/TAZ-LLPS puncta, yellow arrows indicate TAZ/TAZ-LLPS puncta. Low magnification images (left) and enlarged images the area outlined in yellow dotted lines in left panels (right). (*B-C*, *E*, *G*) ***p < 0.001; **p < 0.01; *p < 0.05; n.s., not significant (Welch's T test). n=3 (*B-C*, *G*; biological replicates, *E*; technical replicates). Error bars indicate the mean ± SD. All scale bars represent 10 μm.

Figure 3. Multivalent association between YAP1-2α/TAZ/TEAD complex and BRD4 via the YAP1 WW domain is essential for YAP1 LLPS. *A*, Puncta formation of YAP1-1α and YAP1-2α. Schematic diagrams of YAP1-1α and YAP1-2α (top). The fluorescence signal of mVenus (bottom). *B*, Schematic diagram of BRD4. BRD4 has two WW domain-binding motifs. PPxY or LPxY: WW domain-binding motifs. *C*, Structural prediction of the interaction between YAP1-2α and BRD4 using AlphaFold2. The WW2 domain (grey), LPxY motif (blue), and PPxY motif (magenta) are shown in the ribbon diagram (top). The vacuum electrostatic surface of the WW2 domain is represented in red (acidic) to blue (basic) (middle). The buried surface area of the LPxY and PPxY motifs in the complex (bottom). *D*, Interaction between HA-YAP1-2α and Flag-BRD4 mutants in MDA-MB-436 cells was examined by anti-Flag immunoblotting analysis of anti-HA immunoprecipitates. Total cell lysates (TCL) were put as input samples (left panel). The relative interaction between YAP1-2α

and BRD4 was calculated by defining Flag-BRD4 (WT) intensity per HA-YAP1-2α intensity in the IP sample as one (right panel). *E*, Effect of BRD4 inhibition on mCherry-fused YAP1-2α puncta formation in MDA-MB-436 cells. Cells transfected with shBRD4 were marked by GFP (green). mCherry-fused YAP1-2α (red). The cells indicated by white arrows were magnified, and the number of YAP1-2α puncta in the nucleus was calculated (top right). BRD4 was knocked down using two different shRNAs (#1 and #2) (bottom right). *F*, Genetic rescue of the shBRD4-mediated reduction in YAP1-2α puncta formation by shBRD4-resistant BRD4. YAP1-2α (red), Flag-BRD4 (gray), nuclei (blue). The area indicated by the yellow dashed box is enlarged (bottom). Yellow arrows indicate the colocalization of YAP1-2α puncta and BRD4. *G-H*, The loss-of-function WW domain mutants were created by introducing point mutations into WW domains of YAP1-2α ($WW1^{mut}$: W199A+P202A, $WW2^{mut}$: W258A+P261A, $WW1/2^{mut}$: W199A+P202A|W258A+P261A). The effect of loss-of-function of WW domain in UWB1.289 cells on nuclear YAP1 puncta formation was evaluated by immunofluorescence staining (*G*). The binding ability between YAP1-WW domain mutants and BRD4 was evaluated using PLA (*H*). (*D-E, G-H*) ***$p < 0.001$; **$p < 0.01$; *$p < 0.05$; n.s., not significant (*E*: Student's T test; *D*, *G-H*: Welch's T test). n=3 (*D-E*; biological replicates, *G-H*; technical replicates). Error bars indicate the mean ± SD. All scale bars represent 10 μm.

Figure 4. YAP1-2α/TAZ/TEAD/BRD4 complex accumulates at super-enhancer elements. *A-C*, The expression level of typical TEAD target gene (*CCN1*) was analyzed by qPCR. UWB1.289 cells transduced with the indicated YAP1 isoforms using lentiviruses (*A*). HA-YAP1-2α or empty vector transfected *TAZ*-KO or KO control UWB1.289 cells (*B*). Artificial heterodimerization between YAP1-2α(LZM) and TAZ(LZM), or YAP1-2γ and TAZ(LZM) in UWB1.289 cells using the iDimerize Induceble Heterodimer System, shown as Figure 2*E* (*C*). *D*, Prediction of potential TEAD-positive super-enhancer elements upstream of the *CCN1* gene. The identified super-enhancer elements in serous ovarian cancer cells (GSM3328052: PEO1 cells) and triple-negative breast cancer cells (GSM6132824: MDA-MB-436 cells) are shown in first and second line from the top. The TEAD-binding motif sequences were predicted using JASPR. Potential TEAD-positive super-enhancer elements upstream of *CCN1* gene were indicated as red lines (-0.3 kb or -0.85 kb from TSS). *E*, In UWB1.289 cells where endogenous YAP1 was replaced with HA-YAP1-2α or HA-YAP1-2γ (see Figure 1*C*), the enrichment levels of super-enhancer marker BRD4, HA-tagged YAP1, TAZ, and TEAD at predicted super-enhancer elements were evaluated by qPCR. The DNA templates were prepared using CUT & RUN with the indicated antibodies. *F-G*, Analysis of YAP1-2α/TAZ/TEAD complex binding to the predicted super-enhancer regions in 6xHis-YAP1-2α expressing *YAP1*-KO UWB1.289 cells. The DNA or protein samples were prepared using ChIP-re-chip. Formation

of YAP1-2α/TAZ/TEAD complex in the cells treated with K975 or DMSO was confirmed by immunoblotting following ChIP-re-chip (*F*). Enrichment of YAP1-2α/TAZ/TEAD complex on predicted super-enhancer regions was evaluated by ChIP-re-chip-qPCR analysis (*G*). *H*, The effect of JQ1 treatment on the increase in *CCN1* expression mediated by YAP1-2α was analyzed using qPCR. (*A-C*, *E*, *G-H*) ***p < 0.001; **p < 0.01, *p < 0.05, (*A-B*, *E*, *G-H*: Welch's T test, *C*: Student's T test). n=3 (technical replicates). Error bars indicate the mean ± SD.

Figure 5. Highly expressed YAP1-2α correlates with EMT signature in HGSOC patients. *A-B*, HGSOC patients (n = 425) were divided into the "*YAP1-*$\alpha^{dominant}$" (n = 131), "*YAP1-*$\beta^{dominant}$" (n = 83), "*YAP1-*$\gamma^{dominant}$" (n = 78), and "*YAP1-*$\delta^{dominant}$" (n = 133). Genes whose expression increased in "*YAP1-*$\alpha^{dominant}$" vs. "*YAP1-*$\gamma^{dominant}$" (FDR < 0.1, FC >1.5) or deceased in "*YAP1-*$\alpha^{dominant}$" vs. "*YAP1-*$\gamma^{dominant}$" (FDR < 0.1, FC <1.5) were shown in volcano plot (*A*). Gene-set enrichment analysis of increased genes (Hallmark MSigDB). The size of circle indicates number of enrichment genes. The -log10(FDR) value is represented in blue (high) to red (low)(*B*). *C*, The expression level of EMT/stemness related genes were analyzed by qPCR. UWB1.289 cells transduced with the indicated YAP1 isoforms using lentiviruses were treated with JQ1 or DMSO as a mock control. *SPARC* (left), *ALDH1A3* (center), and *SNAI2* (right). *D*, The effect of JQ1 treatment on the formation of YAP1-2α-LLPS puncta was analyzed using

immunofluorescence staining. Green: HA-tagged YAP1 (left). Number of YAP1 puncta in the nucleus (right). Scale bars represent 10 μm. *E*, In UWB1.289 cells where endogenous YAP1 was replaced with HA-YAP1-2α or HA-YAP1-2γ (see Figure 1*C*), the enrichment levels of super-enhancer marker BRD4, YAP1 (HA-tag), TAZ, and TEAD at potential super-enhancer elements (left: *SPARC*; -0.67 kb from TSS, right: *SPARC*; -3.2 kb from TSS) were evaluated by qPCR. The DNA templates were prepared using CUT & RUN with the indicated antibodies. *F*, *TAZ*-KO or KO control UWB1.289 cells were transfected with HA-YAP1-2α or an empty vector as control. The mRNA expression levels of *SPARC* (left) and *ALDH1A3* (right) were assessed by qPCR. Relative mRNA expression levels were calculated with cells transfected with an empty vector as one. (*C*-*F*) ***p < 0.001; **p < 0.01, *p < 0.05, n.s., not significant (Welch's T test). n=3 (technical replicates). Error bars indicate the mean ± SD.

Figure 6. YAP1-2α strengthens cancer cell robustness and potentiates malignant characteristics. *A*-*B*, Two-dimensional or three-dimensional cell proliferation of YAP1-2α-overexpressing, YAP1-2γ-overexpressing, or control UWB1.289 cells. Two-dimensional cell proliferation was measured by an MTS assay (*A*). Anchorage-independent 3D cell growth was evaluated by detecting ATP content (*B*). *C*, YAP1-2α-overexpressing or control UWB1.289 spheroids were treated with K-975, JQ1, or DMSO as a mock-treated control. Bright-field images and ki-67 staining of 3D-

cultured spheroids. Scale bars represent 100 μm. The Feret diameter of the spheroids is shown in the graph (bottom right). Red bars represent mean values. ***p < 0.001; **p < 0.01 (Welch's T test). *D-E*, YAP1-2α-overexpressing or YAP1-2γ-overexpressing UWB1.289 cells were treated with K-975, JQ1 or DMSO as a mock-treated control, followed by chemotaxis, matrix invasion, or ferroptosis assays. Chemotaxis capacity (*D*, left bottom panel) or matrix invasion ability (*D*, right bottom panel) was analyzed using transwell. Schematic view was shown (*D*, top panels). The number of cells that migrated or invaded into the lower well was measured by detecting ATP content (*D*). Chlorido [N, N'-Disalicylidene-1,2-Phenylenediamine] Iron (III) was used as ferroptosis inducer. Cell viability was measured by detecting ATP content. Relative cell viability was calculated as the ratio of cells treated with ferroptosis inducer to untreated cells within each group (*E*). (*A-B*, *D-E*) ***p < 0.001; **p < 0.01; *p < 0.05; n.s., not significant (*A*, *D-E*: Welch's T test, *B*: Student's T test). n=3 (technical replicates). Error bars indicate mean ± SD. *F-H*, Analysis of sequential tissue sections derived from patients with high-grade serous ovarian cancer. *YAP1-2α* mRNA was visualized using BaseScope and its intensity was quantified using ImageJ software. The correlation between clinical stage and expression levels of *YAP1-2α* mRNA expression levels (BaseScope intensity per cell) is shown in box-and-whisker plots. The Boxes include the 25th–75th percentiles, with bars indicating means and whiskers indicating the range of data. **p < 0.01;

*p < 0.05 (Student's T test) (*F*). BaseScope signals (*YAP1-2α* mRNA) (*G*, left panels), HE staining (*G*, right panel), and YAP1 immunofluorescence staining (*H*) in HGSOC patient with high *YAP1-2α* expression (*YAP1-2α* staining score: 3+). Nuclei were stained with DAPI. The dashed box area was enlarged. Scale bars represent 100 μm.

Figure 1.

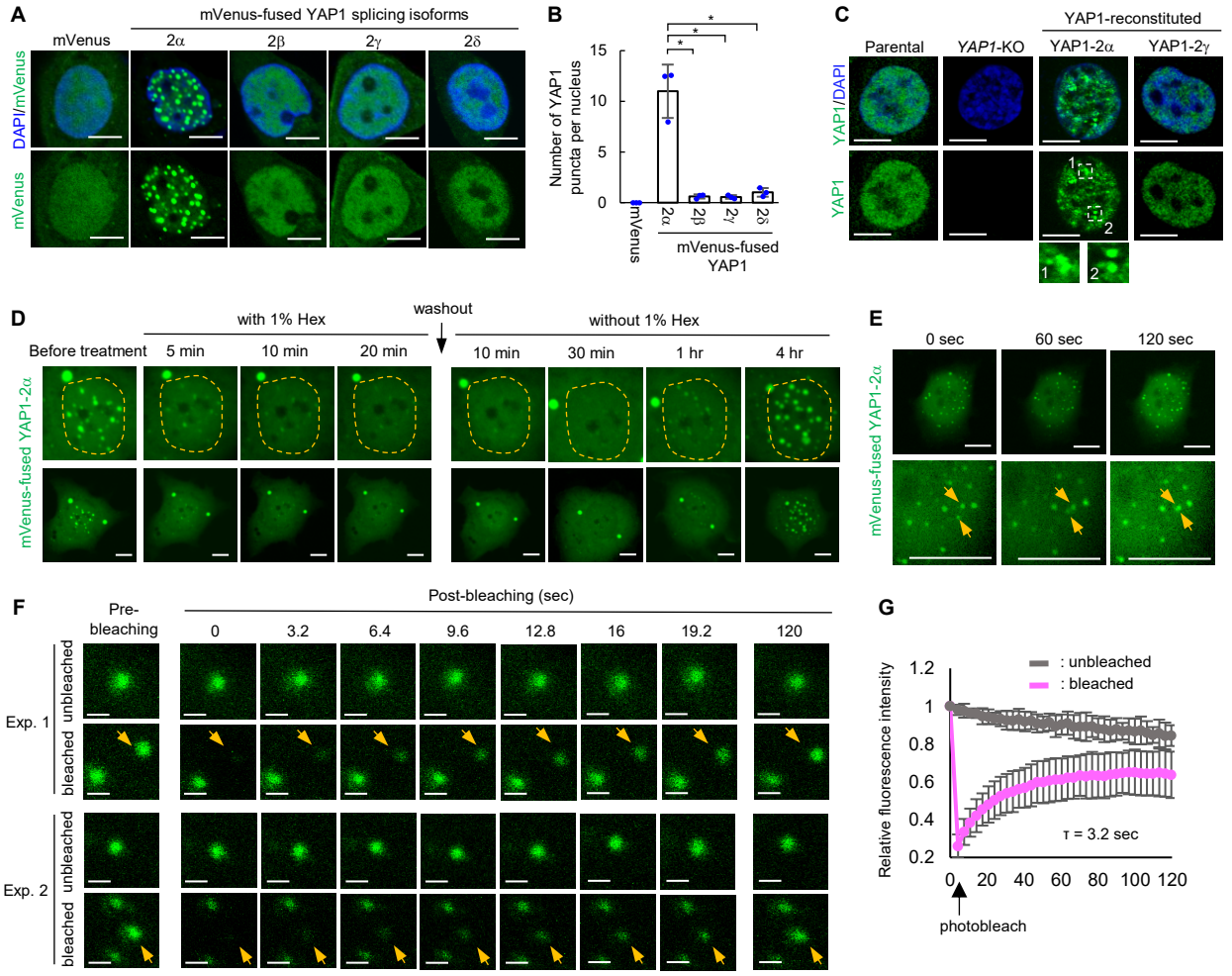
A
mVenus-fused YAP1 splicing isoforms
mVenus
2α
2β
2γ
2δ
DAPI/mVenus
mVenus
B
Number of YAP1 puncta per nucleus
15
10
5
0
mVenus
2α
2β
2γ
2δ
mVenus-fused YAP1
C
YAP1-reconstituted
Parental
YAP1-KO
YAP1-2α
YAP1-2γ
YAP1/DAPI
YAP1
1
2
D
with 1% Hex
washout
without 1% Hex
Before treatment
5 min
10 min
20 min
10 min
30 min
1 hr
4 hr
mVenus-fused YAP1-2α
E
0 sec
60 sec
120 sec
mVenus-fused YAP1-2α
F
Pre-bleaching
Post-bleaching (sec)
0
3.2
6.4
9.6
12.8
16
19.2
120
Exp. 1
Exp. 2
unbleached
bleached
G
: unbleached
: bleached
Relative fluorescence intensity
1.2
1
0.8
0.6
0.4
0.2
τ = 3.2 sec
0
20
40
60
80
100
120
photobleach

Figure 2.

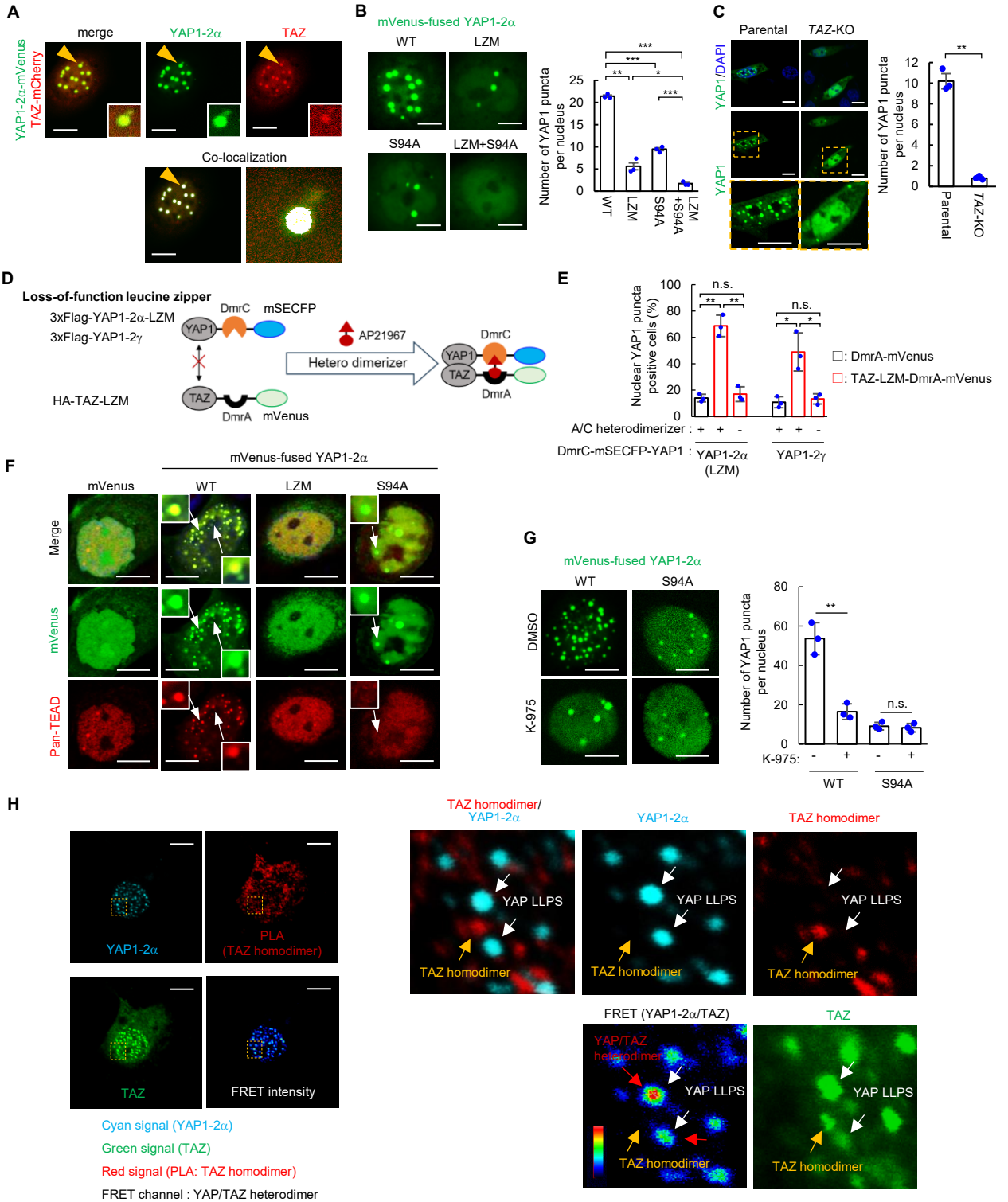
A
merge
YAP1-2α
TAZ
YAP1-2α-mVenus
TAZ-mCherry
Co-localization
B
mVenus-fused YAP1-2α
WT
LZM
S94A
LZM+S94A
Number of YAP1 puncta per nucleus
C
Parental
TAZ-KO
YAP1/DAPI
YAP1
Number of YAP1 puncta per nucleus
D
Loss-of-function leucine zipper
3xFlag-YAP1-2α-LZM
3xFlag-YAP1-2γ
HA-TAZ-LZM
DmrC
mSECFP
YAP1
TAZ
DmrA
mVenus
AP21967
Hetero dimerizer
E
Nuclear YAP1 puncta positive cells (%)
n.s.
□: DmrA-mVenus
□: TAZ-LZM-DmrA-mVenus
A/C heterodimerizer :
DmrC-mSECFP-YAP1 :
YAP1-2α (LZM)
YAP1-2γ
F
mVenus-fused YAP1-2α
mVenus
WT
LZM
S94A
Merge
mVenus
Pan-TEAD
G
mVenus-fused YAP1-2α
WT
S94A
DMSO
K-975
Number of YAP1 puncta per nucleus
K-975:
H
YAP1-2α
PLA (TAZ homodimer)
TAZ
FRET intensity
Cyan signal (YAP1-2α)
Green signal (TAZ)
Red signal (PLA: TAZ homodimer)
FRET channel : YAP/TAZ heterodimer
TAZ homodimer/ YAP1-2α
YAP1-2α
TAZ homodimer
YAP LLPS
TAZ homodimer
FRET (YAP1-2α/TAZ)
YAP/TAZ heterodimer
TAZ

Figure 3.

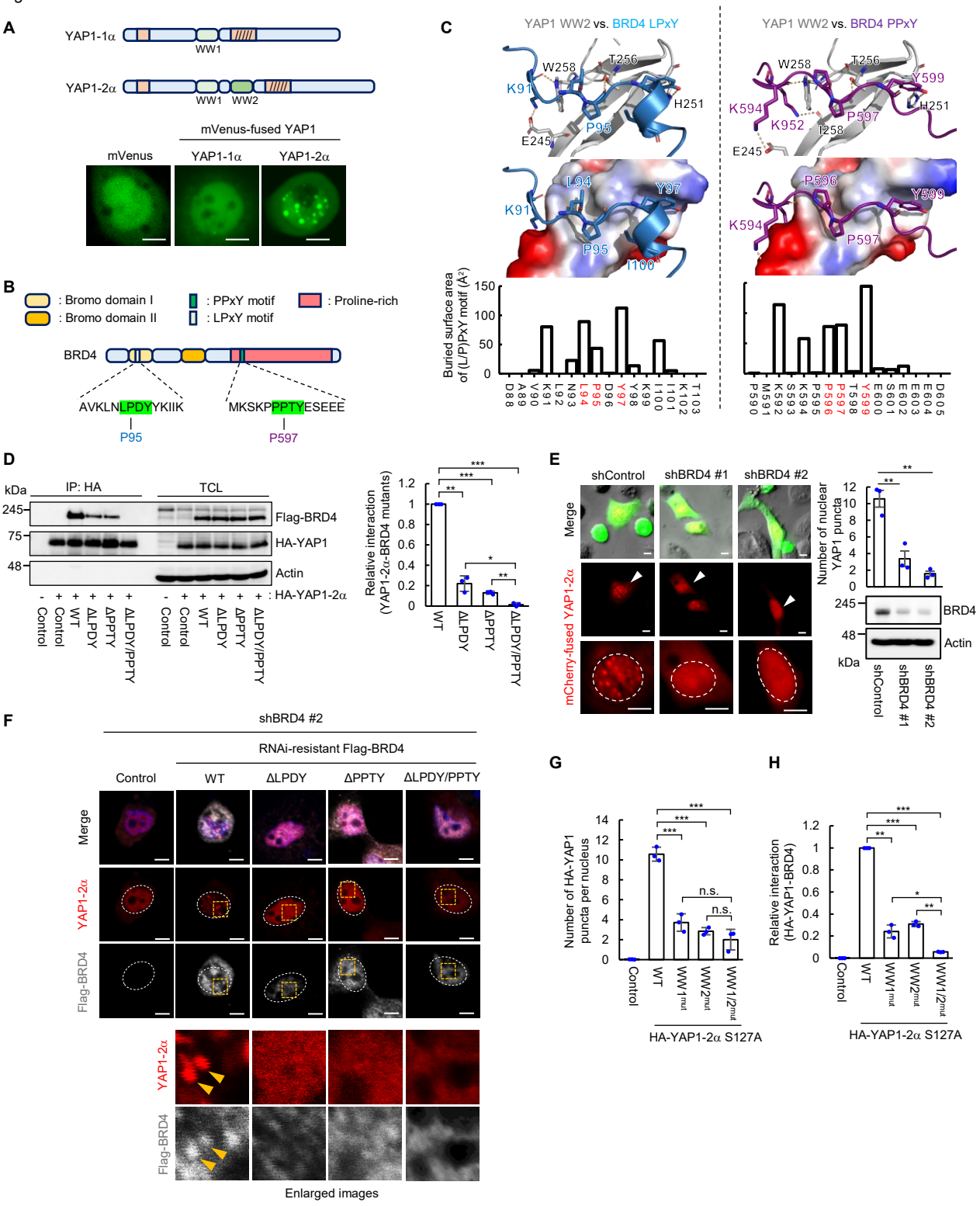
A
YAP1-1α
WW1
YAP1-2α
WW1 WW2
mVenus-fused YAP1
mVenus
YAP1-1α
YAP1-2α
B
: Bromo domain I
: Bromo domain II
: PPxY motif
: LPxY motif
: Proline-rich
BRD4
AVKLNLPDYYKIIK
MKSKPPPTYESEEE
P95
P597
C
YAP1 WW2 vs. BRD4 LPxY
YAP1 WW2 vs. BRD4 PPxY
Buried surface area of (L/P)PxY motif (Å²)
D
kDa
IP: HA
TCL
Flag-BRD4
HA-YAP1
Actin
: HA-YAP1-2α
Control
WT
ΔLPDY
ΔPPTY
ΔLPDY/PPTY
Relative interaction (YAP1-2α-BRD4 mutants)
E
shControl
shBRD4 #1
shBRD4 #2
Merge
mCherry-fused YAP1-2α
Number of nuclear YAP1 puncta
BRD4
Actin
F
shBRD4 #2
RNAi-resistant Flag-BRD4
Control
WT
ΔLPDY
ΔPPTY
ΔLPDY/PPTY
Merge
YAP1-2α
Flag-BRD4
Enlarged images
G
Number of HA-YAP1 puncta per nucleus
n.s.
HA-YAP1-2α S127A
H
Relative interaction (HA-YAP1-BRD4)
HA-YAP1-2α S127A

Figure 4.

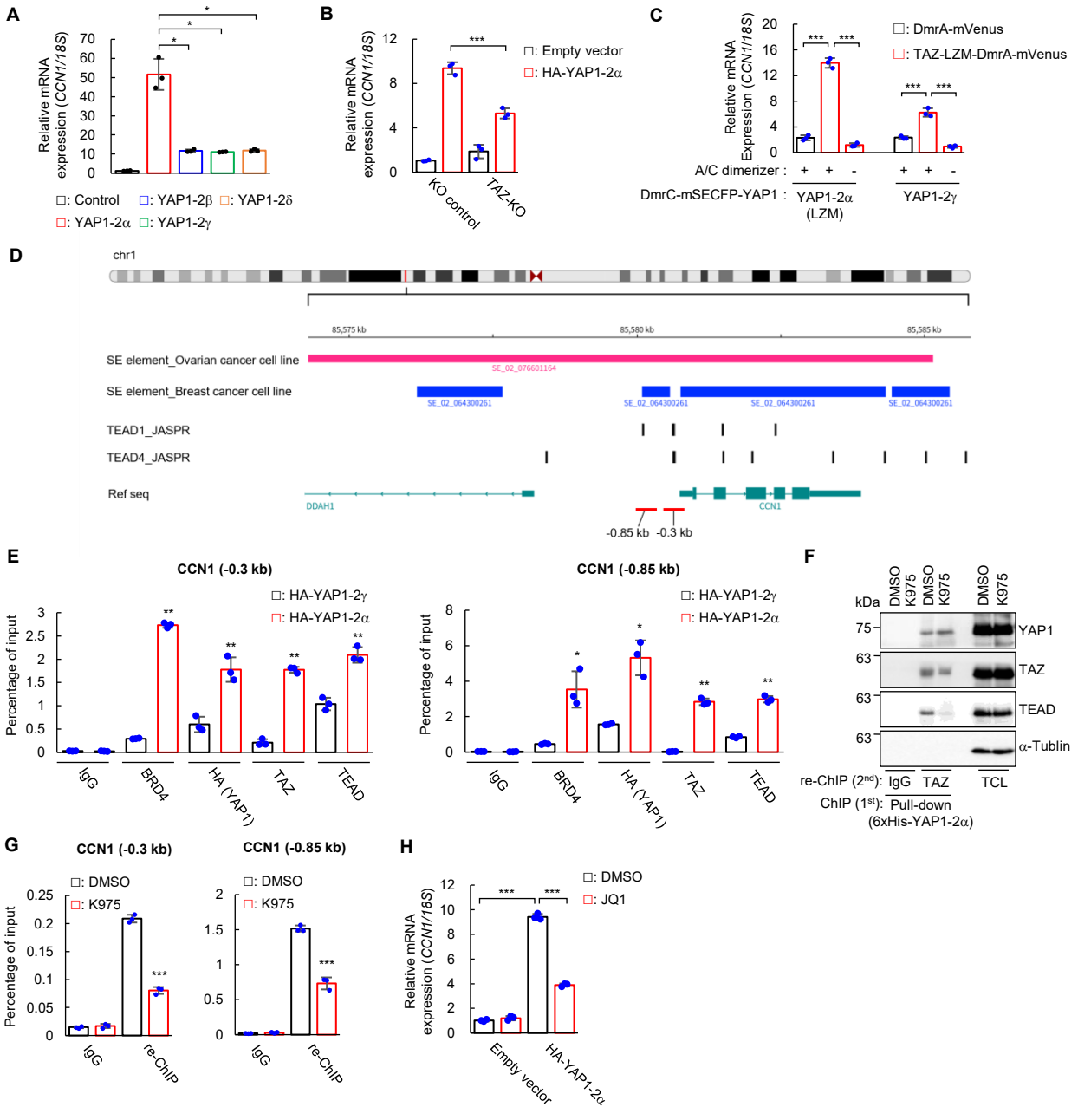
A
Relative mRNA expression (CCN1/18S)
□: Control □: YAP1-2β □: YAP1-2δ
□: YAP1-2α □: YAP1-2γ
B
Relative mRNA expression (CCN1/18S)
□: Empty vector
□: HA-YAP1-2α
KO control
TAZ-KO
C
Relative mRNA Expression (CCN1/18S)
□: DmrA-mVenus
□: TAZ-LZM-DmrA-mVenus
A/C dimerizer :
DmrC-mSECFP-YAP1 :
YAP1-2α (LZM)
YAP1-2γ
D
chr1
85,575 kb
85,580 kb
85,585 kb
SE element_Ovarian cancer cell line
SE element_Breast cancer cell line
TEAD1_JASPR
TEAD4_JASPR
Ref seq
DDAH1
CCN1
-0.85 kb
-0.3 kb
E
CCN1 (-0.3 kb)
CCN1 (-0.85 kb)
□: HA-YAP1-2γ
□: HA-YAP1-2α
Percentage of input
IgG
BRD4
HA (YAP1)
TAZ
TEAD
F
kDa
DMSO
K975
YAP1
TAZ
TEAD
α-Tublin
re-ChIP (2nd): IgG TAZ TCL
ChIP (1st): Pull-down (6xHis-YAP1-2α)
G
CCN1 (-0.3 kb)
CCN1 (-0.85 kb)
□: DMSO
□: K975
Percentage of input
IgG
re-ChIP
H
Relative mRNA expression (CCN1/18S)
□: DMSO
□: JQ1
Empty vector
HA-YAP1-2α

Figure 5.

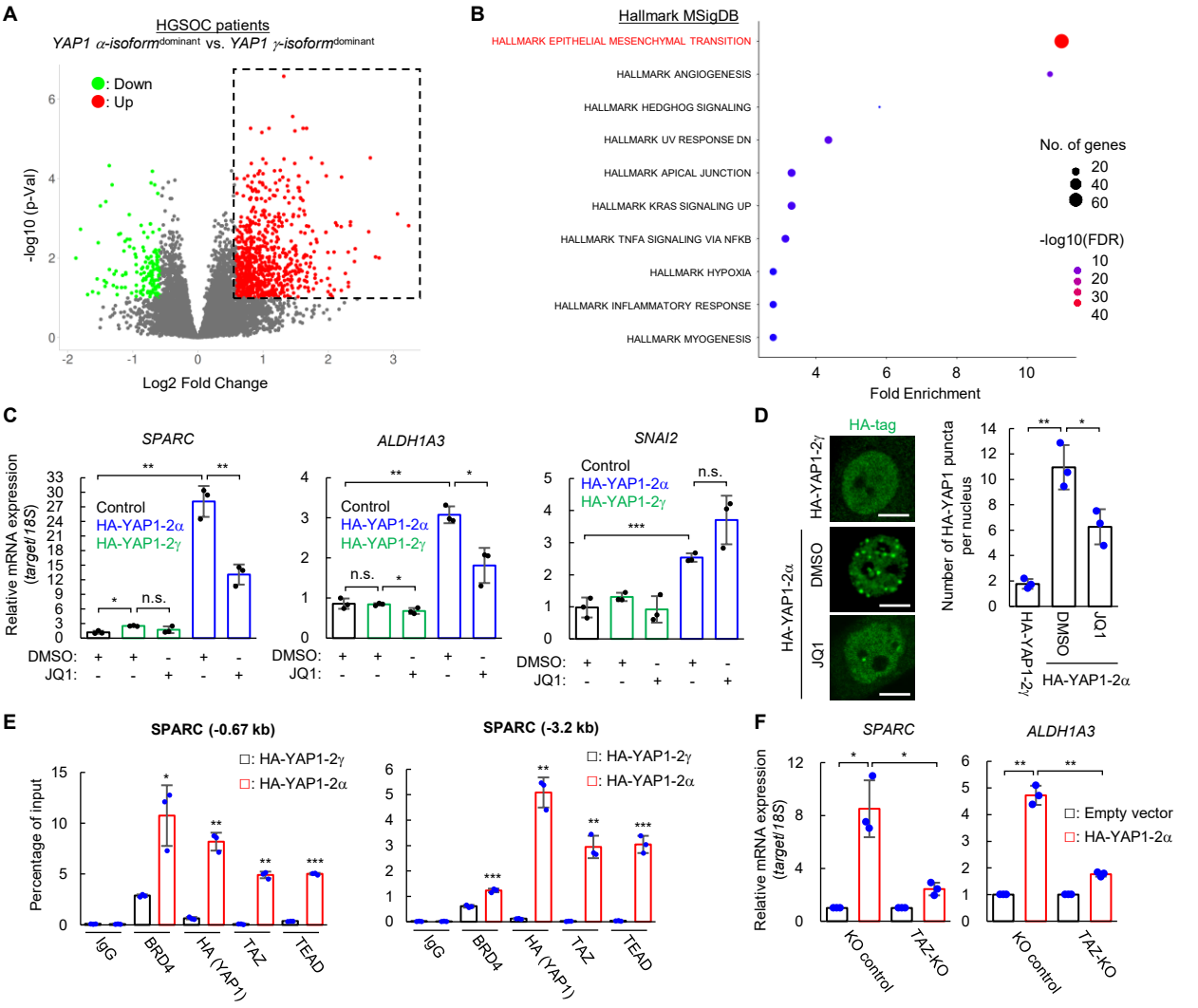
A
HGSOC patients
YAP1 α-isoformdominant vs. YAP1 γ-isoformdominant
: Down
: Up
-log10 (p-Val)
Log2 Fold Change
B
Hallmark MSigDB
HALLMARK EPITHELIAL MESENCHYMAL TRANSITION
HALLMARK ANGIOGENESIS
HALLMARK HEDGHOG SIGNALING
HALLMARK UV RESPONSE DN
HALLMARK APICAL JUNCTION
HALLMARK KRAS SIGNALING UP
HALLMARK TNFA SIGNALING VIA NFKB
HALLMARK HYPOXIA
HALLMARK INFLAMMATORY RESPONSE
HALLMARK MYOGENESIS
Fold Enrichment
No. of genes
-log10(FDR)
C
SPARC
ALDH1A3
SNAI2
Relative mRNA expression (target/18S)
Control
HA-YAP1-2α
HA-YAP1-2γ
DMSO:
JQ1:
n.s.
D
HA-tag
HA-YAP1-2γ
HA-YAP1-2α
DMSO
JQ1
Number of HA-YAP1 puncta per nucleus
E
SPARC (-0.67 kb)
SPARC (-3.2 kb)
□: HA-YAP1-2γ
□: HA-YAP1-2α
Percentage of input
IgG
BRD4
HA (YAP1)
TAZ
TEAD
F
SPARC
ALDH1A3
Relative mRNA expression (target/18S)
□: Empty vector
□: HA-YAP1-2α
KO control
TAZ-KO

Figure 6.

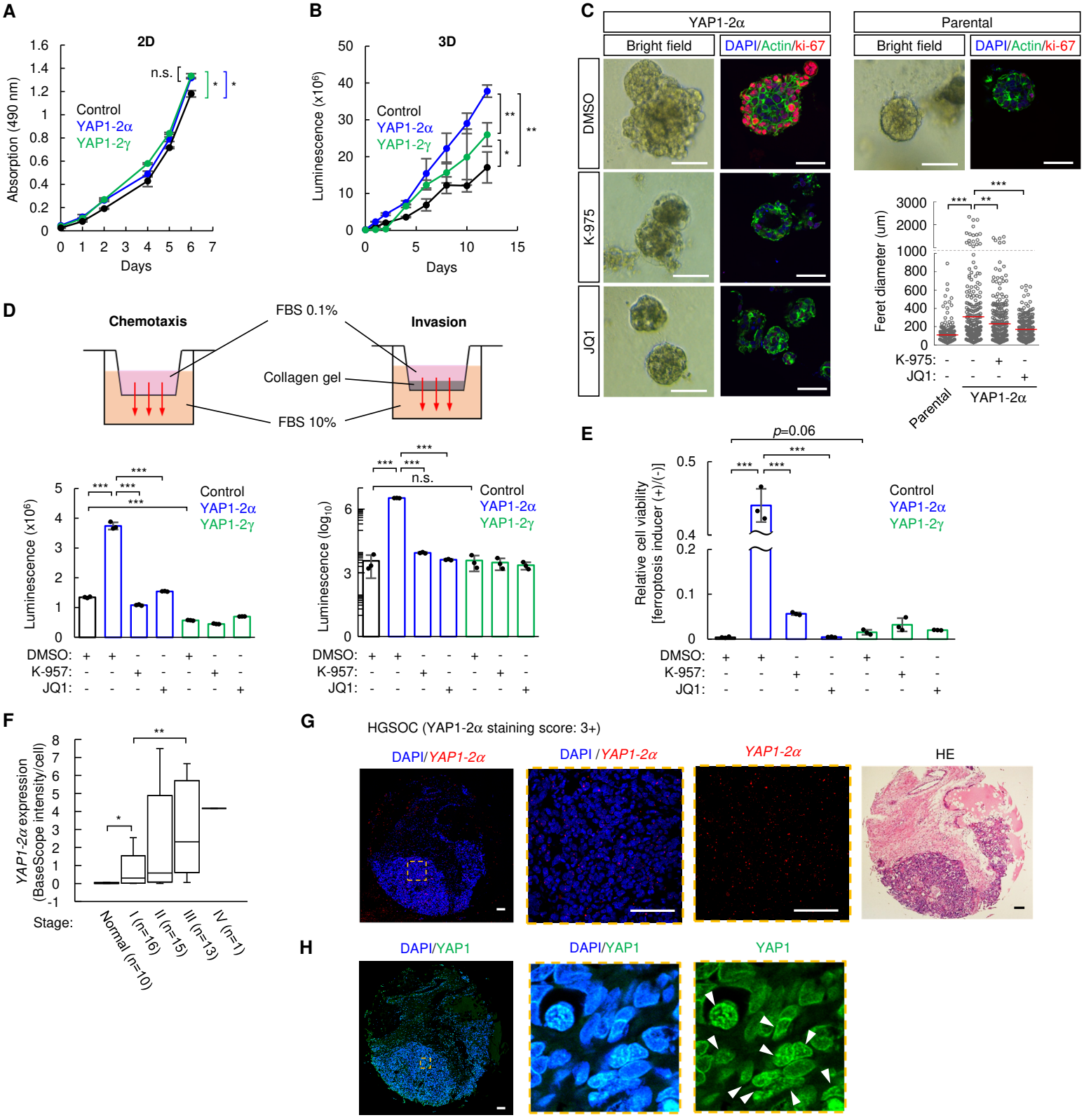
A
2D
Absorption (490 nm)
Days
Control
YAP1-2α
YAP1-2γ
n.s.
B
3D
Luminescence (x10^6)
Days
C
YAP1-2α
Parental
Bright field
DAPI/Actin/ki-67
DMSO
K-975
JQ1
Feret diameter (um)
K-975:
JQ1:
Parental
YAP1-2α
D
Chemotaxis
Invasion
FBS 0.1%
Collagen gel
FBS 10%
Luminescence (x10^6)
Luminescence (log10)
DMSO:
K-957:
JQ1:
E
p=0.06
Relative cell viability [ferroptosis inducer (+)/(-)]
F
YAP1-2α expression (BaseScope intensity/cell)
Stage:
Normal (n=10)
I (n=16)
II (n=15)
III (n=13)
IV (n=1)
G
HGSOC (YAP1-2α staining score: 3+)
DAPI/YAP1-2α
DAPI /YAP1-2α
YAP1-2α
HE
H
DAPI/YAP1
DAPI/YAP1
YAP1

The YAP1 isoform, YAP1-2α, promotes oncogenic properties by inducing liquid-liquid phase separation through specific heterodimerization with TAZ

Takuya Ooki[1], Takeru Hayashi[1], Yui Yamamoto[1], & Masanori Hatakeyama[1,2,*]

[1]Laboratory of Microbial Carcinogenesis, Institute of Microbial Chemistry, Microbial Chemistry Research Foundation, Tokyo, Japan

[2]Center of Infection-associated Cancer, Institute for Genetic Medicine, Hokkaido University, Sapporo, Japan

*e-mail: mhata@m.u-tokyo.ac.jp

Running title

Molecular Mechanism of LLPS Induction by YAP isoform YAP1-2α

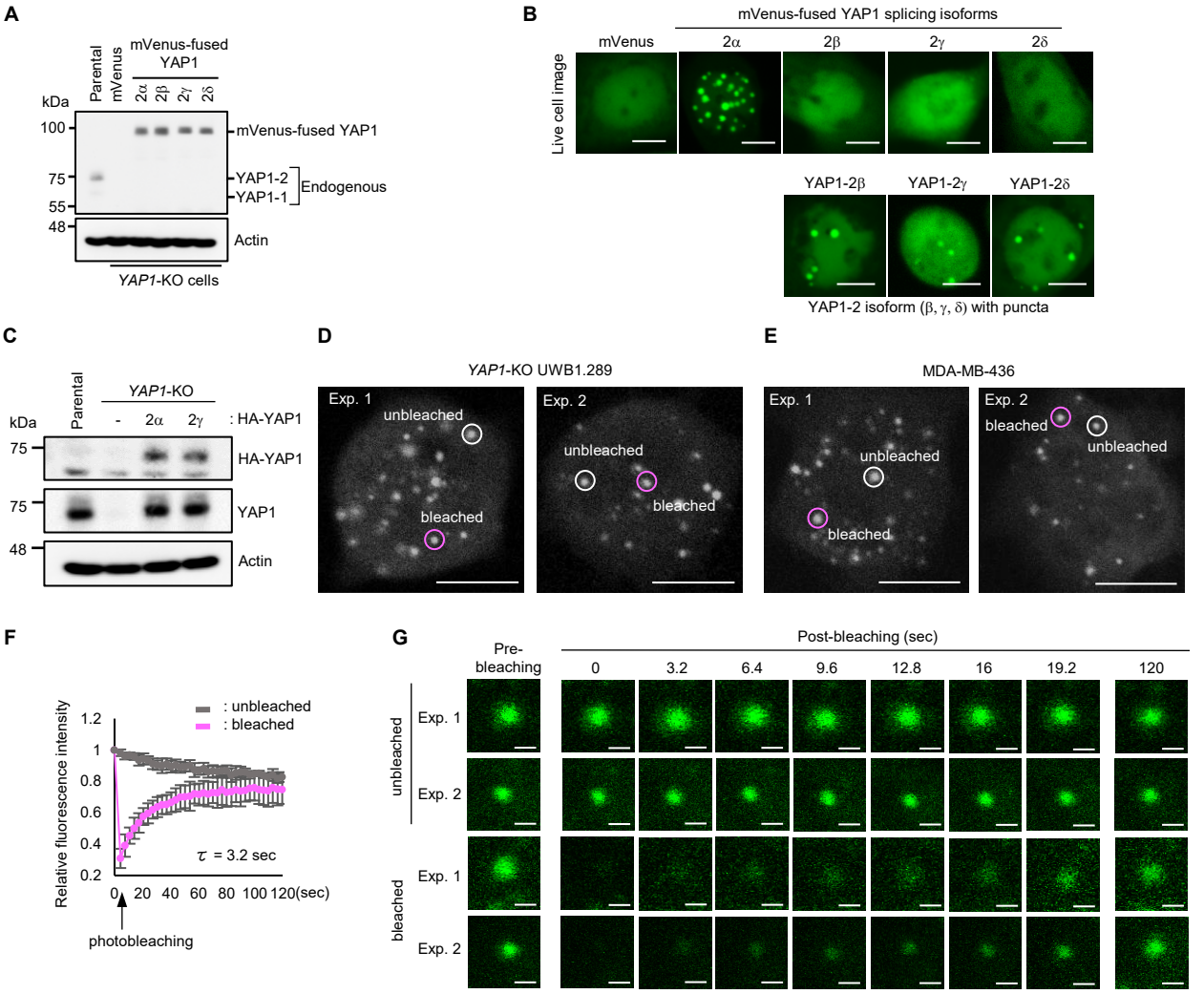

Figure S1. YAP1-2α induces LLPS.
A, Immunoblotting of endogenous YAP1-1, YAP1-2, and mVenus-fused YAP1 isoforms (related to Fig. 1*A*-*B*). *B*, Live cell imaging analysis of *YAP1*-KO UWB1.289 cells transfected with indicated mVenus-fused YAP1 isoform plasmids. Fluorescence of mVenus was detected as a green signal. Although very rare, a few puncta-positive cells were present in cells expressing mVenus-fused YAP1-2β, γ, or δ (shown in the bottom three panels). *C*, Immunoblotting analysis using indicated antibodies (related to Fig. 1*C*). *D*, Entire nuclear images of cells used for FRAP analysis (related to Fig. 1*F*). Two different cells were labeled as Exp. 1 and Exp. 2. White circles indicate non-photobleached puncta. The pink circles indicate photobleached puncta. *E*-*G*, FRAP analysis of MDA-MB-436 cells expressing mVenus-fused YAP1-2α. Entire nuclear images of cells used for FRAP analysis (*E*). Fluorescence intensities of puncta (photobleached; n=5, unbleached; n=5) obtained from a series of time-lapse images were analyzed. τ indicates interval of fluorescence detection. Error bars indicate mean ± SD (*F*). Representative time-lapse images. Scale bars indicate 1 μm (*G*). (*B*, *D*-*E*) Scale bars indicate 10 μm.

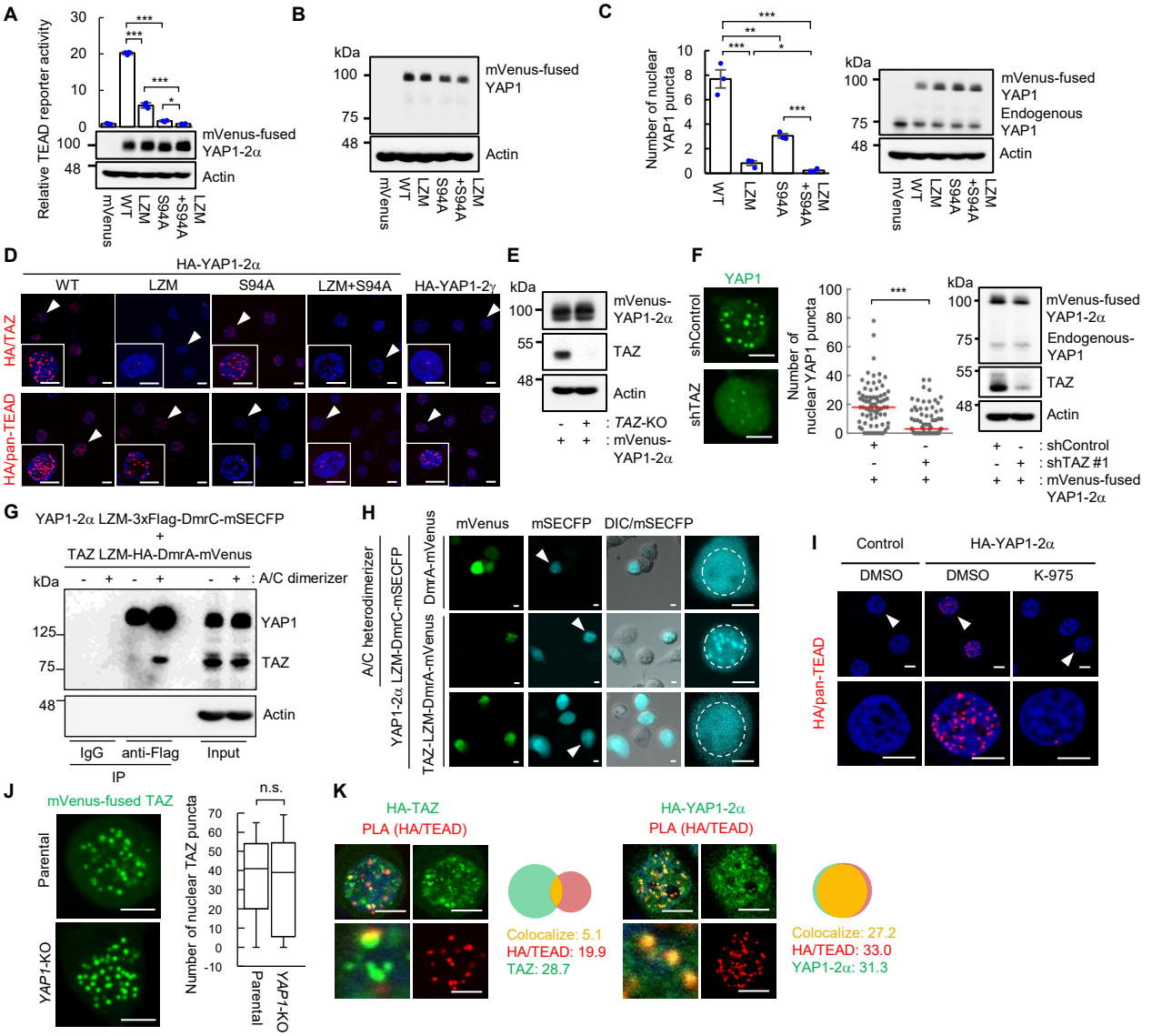

Figure S2. The YAP1-2α/TAZ/TEAD enhancer complex is required for LLPS formation

A, TEAD reporter assay of YAP1-2α mutants in *YAP1*-KO UWB1.289 cells (top). Expression of the YAP1-2α mutant proteins (bottom). *B*, The expression of the indicated proteins in *YAP1*-KO UWB1.289 cells was confirmed by immunoblotting (related to Fig. 2*B*). *C*, The nuclear puncta formation in MDA-MB-436 cells expressing mVenus-fused YAP1-2α mutants. The number of YAP1 puncta in the nucleus (left). Protein expression shown by immunoblotting (right). *D*, Interaction of YAP1-2α with endogenous TAZ (top) or TEAD (bottom) in UWB1.289 cells was visualized as PL spots (red) using PLA. The nuclei indicated by white arrows are magnified. *E*, mVenus-fused YAP1-2α expression in *TAZ*-KO MDA-MB-436 cells were confirmed by immunoblotting. *F*, UWB1.289 cells stably expressing shRNA targeting *TAZ* mRNA were transfected with an mVenus-fused YAP1-2α vector. Fluorescence images (left). Number of YAP1-2α puncta in the nucleus. Bars indicate medians, n=75 cells per group were obtained from three biological replicate experiments, respectively (center). Confirmation of TAZ knockdown and mVenus-fused YAP1-2α expression by immunoblotting (right). *G-H*, related to Fig. 2*D-E*. Confirmation of heterodimer formation between indicated proteins upon treatment with heterodimerizer (*G*) and immunofluorescence images (*H*). DIC: differential interference contrast image. *I*, Inhibition of the physical interaction between HA-YAP1-2α and endogenous TEAD by K-975 in UWB1.289 cells was detected using PLA. *J*, Effect of *YAP1* knockout on TAZ/TAZ LLPS in UWB1.289 cells. TAZ/TAZ LLPS (left). Number of nuclear TAZ puncta in Parental or *YAP1*-KO cells (right). Boxes include 25th–75th percentiles with bars indicating medians. n=13 cells for each group. *K*, Interaction of YAP1-2α or TAZ with TEAD in UWB1.289 cells was visualized using PLA following immunofluorescence staining. Co-localization of PL spots and YAP1-2α or TAZ puncta. Green circle: number of YAP1-2α or TAZ puncta, Red circle: number of nuclear PL spots, Yellow circle: number of colocalized spots. n=15 nuclei. All scale bars represent 10 μm. (*A*, *C*, *F*, *J*) ***p < 0.001; **p < 0.01; *p < 0.05; n.s., not significant (*A*, *C*: Student's t test; *F*, *J*: Mann-Whitney U test). (*A*, *C*) Error bars indicate the mean ± SD, n=3 (*A*; technical replicates, *C*; biological replicates).

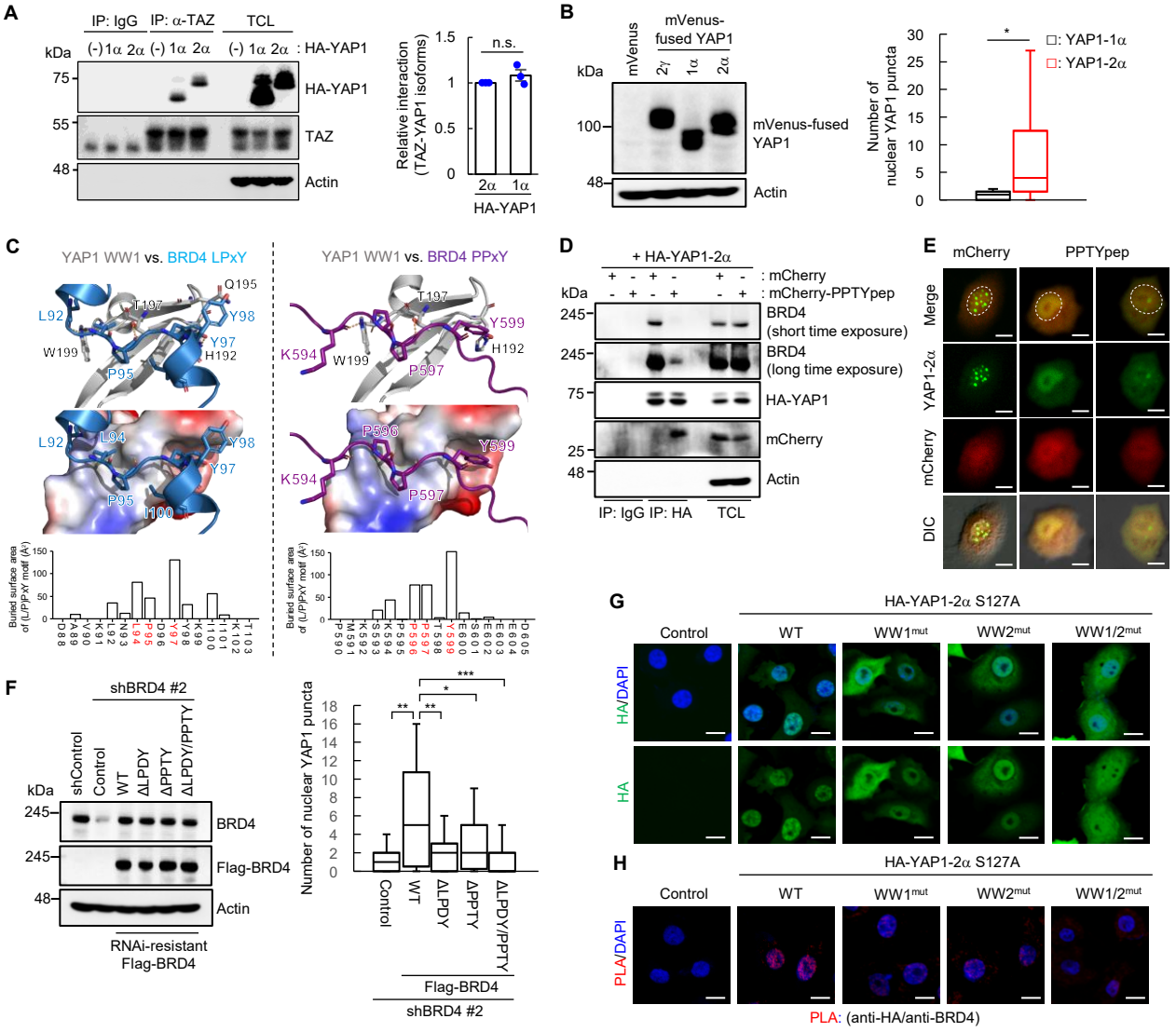

Figure S3. WW domain-mediated multiple interaction between YAP1-2α and BRD4 is important for YAP1 LLPS formation

A, Interactions between TAZ and YAP1-1α or YAP1-2α in MDA-MB-436 cells were examined by an anti-HA immunoblotting analysis of the anti-TAZ immunoprecipitates (left). The relative interaction between YAP1-1α and TAZ was calculated by defining YAP1-2α intensity per TAZ intensity in the IP sample as one (right). n=3 (biological replicates), n.s., not significant (Student's t test). Error bars indicate SEM. *B*, Related to Fig. 3*A*. Expression levels of mVenus-fused YAP1-1α and YAP1-2α were determined by immunoblotting (left). Number of nuclear YAP1 puncta in mVenus-fused YAP1-1α or YAP1-2α expressing cells (right). Boxes include 25th–75th percentiles with bars indicating medians. n=13 cells for each group. *$p < 0.05$ (Welch's t test). *C*, Predicted interaction structure of the WW1 domain of YAP1-2α with BRD4 LPxY or PPxY motif using AlphaFold2. The WW1 domain (gray), LPxY motif (blue), and PPxY motif (magenta) in each rank 1 structure are shown in the ribbon diagram (top). The vacuum electrostatic surface of the WW1 domain is represented in red (acidic) to blue (basic) (middle). The buried surface area of the LPxY and PPxY motif in the complex was estimated (bottom). The polar contacts are indicated by the orange dashed lines. *D*, Competitive inhibition of the YAP1-2α/BRD4 interaction using mCherry-fused PPTY peptide derived from BRD4 sequence (PPTYpep). HA-YAP1-2α-expressing cells were transfected with the mCherry or PPTYpep vector and subjected to a sequential immunoprecipitation-immunoblotting experiment using the indicated antibodies. *E*, Inhibition of YAP1-2α puncta formation using PPTYpep, which interferes the YAP1-2α/BRD4 interaction. *F*, Rerated to Fig. 3*F*. Confirmation of shBRD4 (#2)-resistant Flag-BRD4 mutants and BRD4 knockdown efficiency in MDA-MB-436 cells using immunoblotting (left). The number of YAP1-2α puncta in the nucleus (right). Boxes include 25th–75th percentiles with bars indicating medians. n=20 cells for each group. ***$p < 0.001$; **$p < 0.01$; *$p < 0.05$ (Welch's T test). *G*, Immunofluorescence images in Fig. 3*G*. Green: HA-YAP1, blue: nucleus. *H*, PLA images in Fig. 3*H*. Red dots: PL spots (HA-YAP1/BRD4 interaction), blue: nucleus. All scale bars represent 10 μm.

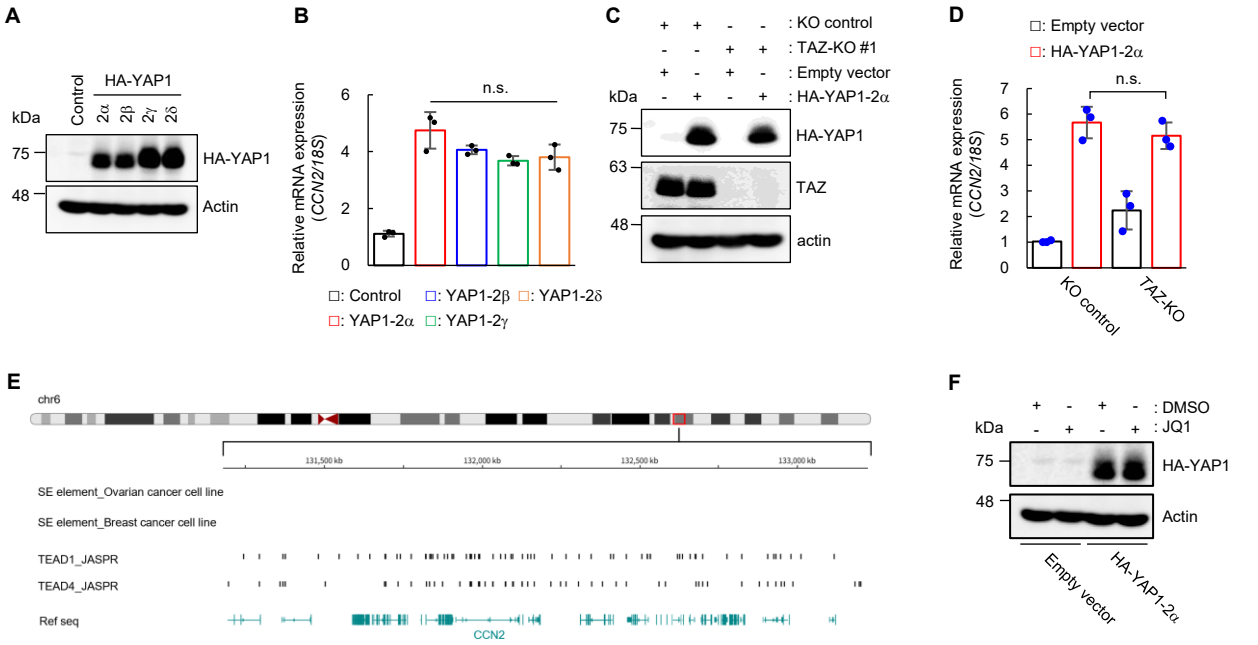

Figure S4. YAP1-2α regulates gene expression in a heterodimerization-dependent manner with TAZ

A-*B*, Related to Fig. 4*A*. Protein expression levels of the HA-YAP1 isoforms were detected by immunoblotting (*A*). The expression level of typical TEAD target gene (*CCN2*) was analyzed by qPCR (*B*). *C*-*D*, Related to Fig. 4*B*. Protein expression levels of the HA-YAP1-2α and TAZ knockout were confirmed by immunoblotting (*C*). The expression level of typical TEAD target gene (*CCN2*) was analyzed by qPCR (*D*). *E*, Prediction of potential TEAD-binding super-enhancer elements around the *CCN2* gene. The identified super-enhancer elements in serous ovarian cancer cells (GSM3328052: PEO1 cells) and triple-negative breast cancer cells (GSM6132824: MDA-MB-436 cells) are shown in first and second line from the top. The TEAD-binding motif sequences were predicted using JASPR. There are no potential TEAD-positive super-enhancer elements in the vicinity of the *CCN2* gene. *F*, related to Fig. 4*H*. Protein expression levels of the HA-YAP1-2α was confirmed by immunoblotting. (*B*, *D*) n.s., not significant (Welch's t test). Error bars indicate the mean ± SD, n=3 (technical replicates).

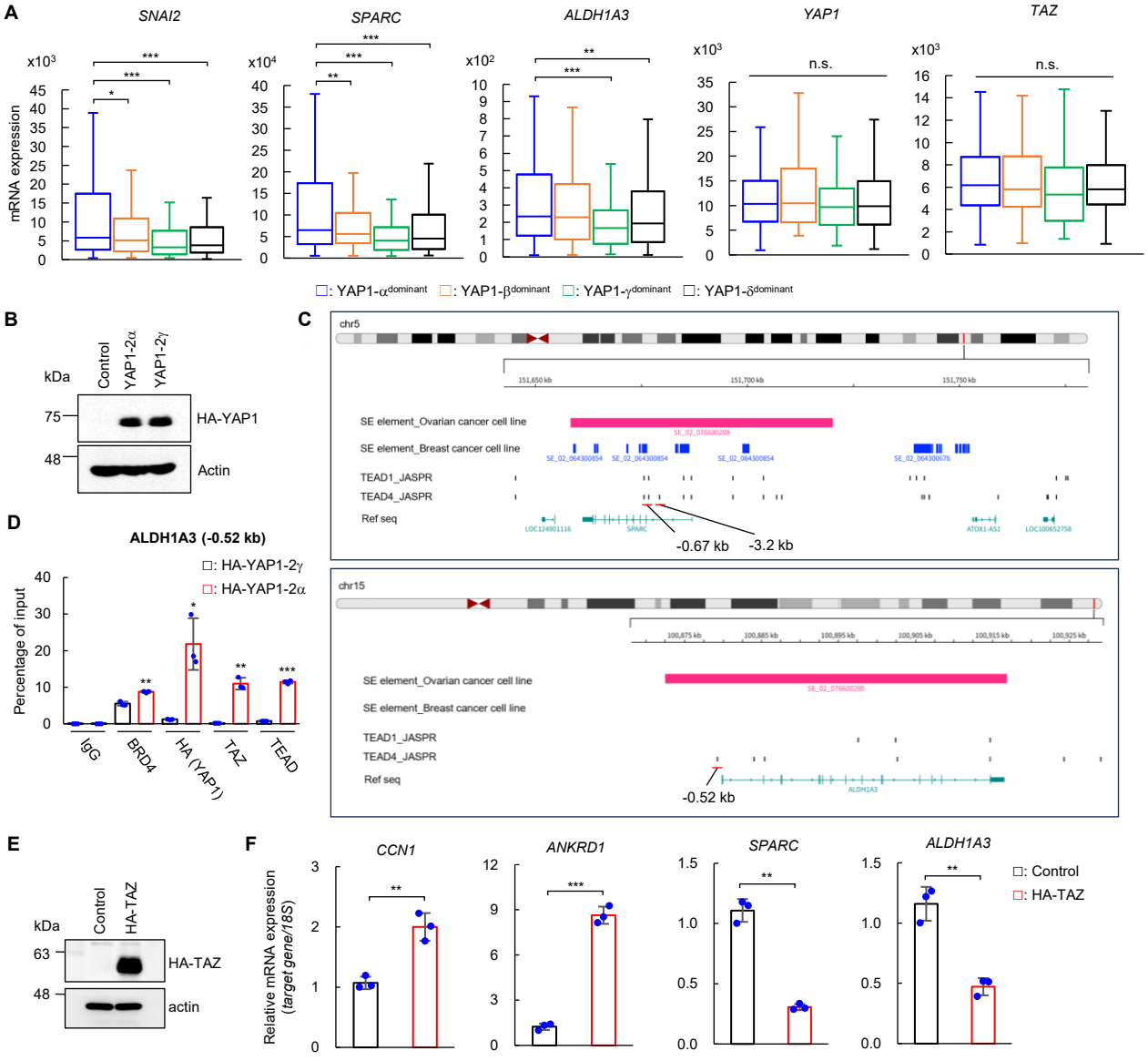

Figure S5. YAP1-2α/TAZ/TEAD super-enhancer activates EMT related genes.
A, Related to Fig. 5*A*-*B*. The mRNA expression levels of EMT related genes (*ZEB1*, *SNAI2*, *SPARC*, *ALDH1A3*), *YAP1*, and *TAZ* in HGSOC patients subdivided by YAP1 isoforms are shown in box-and-whisker plots. The Boxes include the 25th–75th percentiles, with bars indicating means and whiskers indicating the range of data. ***p < 0.001; **p < 0.01; *p < 0.05; n.s., not significant (Welch's t test). *B*, UWB1.289 cells transduced with the indicated YAP1 isoforms using lentiviruses. Protein expression levels of the HA-YAP1 isoforms were detected by immunoblotting. *C*, The identified super-enhancer elements in serous ovarian cancer cells (GSM3328052) and triple-negative breast cancer cells (GSM6132824) are shown in first and second line from the top. The TEAD-binding motif sequences were predicted using JASPR. Upstream of *SPARC* (top panel), and upstream of *ALDH1A3* (bottom panel). The region where primers for ChIP-qPCR were designed is indicated by a red lines. *D*, Related to Fig. 5*E*. The enrichment levels of super-enhancer marker BRD4, YAP1 (HA-tag), TAZ, and TEAD in the potential super-enhancer element upstream of *ALDH1A3*, indicated by the red line in panel *C* (bottom panel), were evaluated using qPCR. The DNA templates were prepared using CUT & RUN with the indicated antibodies. *E*-*F*, Over expression of TAZ in UWB1.289 cells. Immunoblotting analysis using indicated antibodies (*E*). Verifying the effects of TAZ overexpression through qPCR analysis of typical TEAD target genes (*CCN1*, *ANKRD1*), *SPARC*, and *ALDH1A3* (*F*). (*D*, *F*) ***p < 0.001; **p < 0.01, *p < 0.05 (Welch's T test). Error bars indicate the mean ± SD. n=3 (technical replicates).

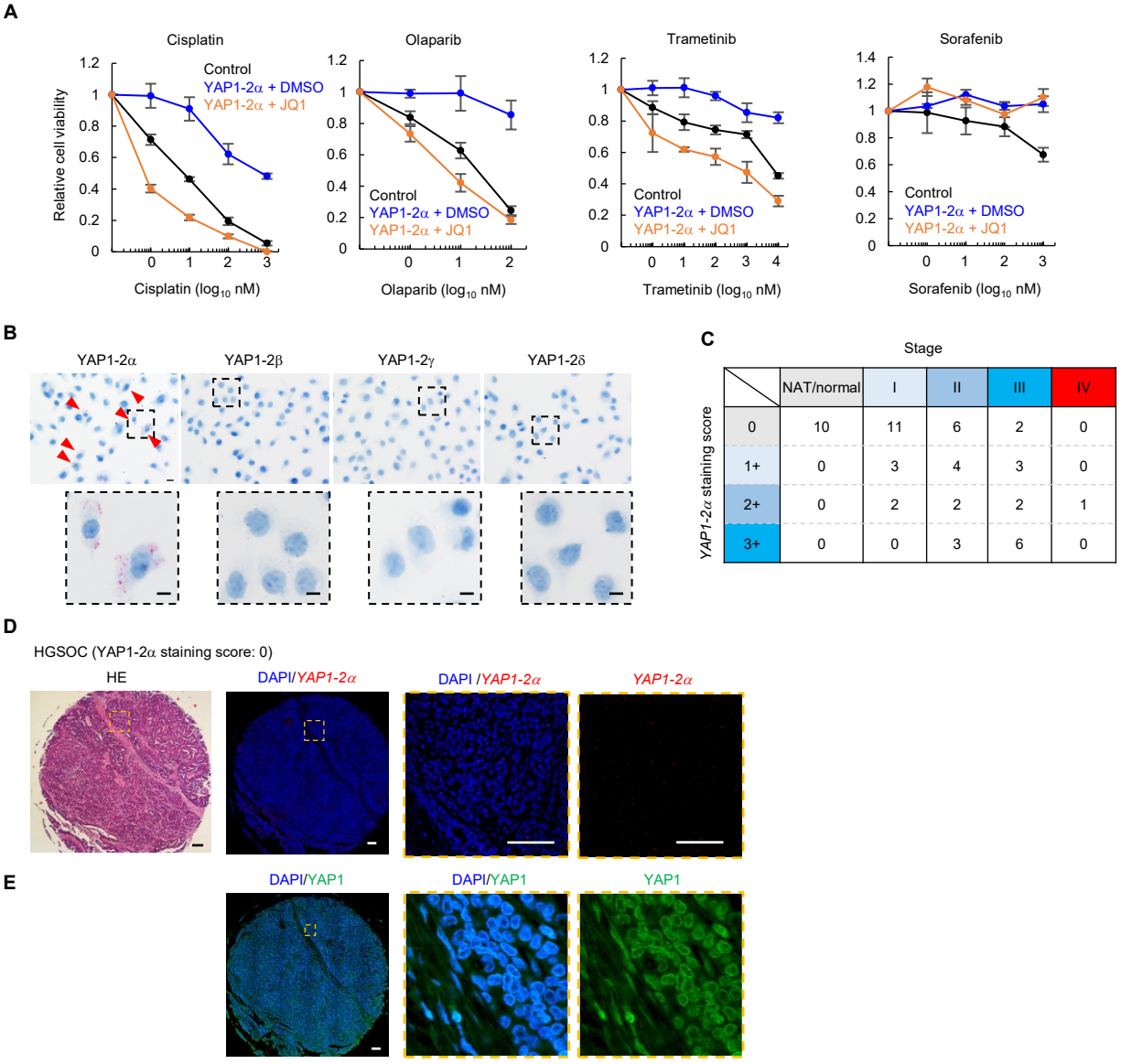

Figure S6. YAP1-2α contributes to acquisition of cancer malignant properties.
A, The effect of the YAP1-2α/TAZ/TEAD super-enhancer on the sensitivity of UWB1.289 cells to various anticancer drugs. Cells were treated with JQ1 along with listed reagent. As mock control, cells were treated with DMSO. Cisplatin, Olaparib (PARP inhibitor), Trametinib (MEK inhibitor), and Sorafenib (tyrosine kinase inhibitor). *B*, Confirmation of BaseScope probe specificity for the *YAP1-2α* isoform. BaseScope was performed in cells transfected with the indicated YAP1 isoforms. Red arrows indicate BaseScope signal-positive cells. *C*, Table of tumor progression stage and *YAP1-2α* staining score. *D-E*, HE staining (*D*, left panel), BaseScope signals (*YAP1-2α* mRNA) (*D*, right panels), and YAP1 immunofluorescence staining (*E*) in HGSOC patient with low *YAP1-2α* expression (*YAP1-2α* staining score: 0). Nuclei were stained with DAPI. The dashed box area was enlarged. Scale bars represent 100 μm.

Table S1. Primer sequences for qRT-PCR

Gene name	Primer sequence
Human *CCN1* Forward	5'-CTCACTGAAGCGGCTCCCTGTTTT-3'
Human *CCN1* Reverse	5'-GGGTTTCTTTCACAAGGCGGCACT-3'
Human *CCN2* Forward	5'-GTGTGACGAGCCCAAGGACCAAAC-3'
Human *CCN2* Reverse	5'-GAGGCGTTGTCATTGGTAACCCGG-3'
Human *ANKRD1* Forward	5'-TGCTTGAATCCACAGCCATCCACT-3'
Human *ANKRD1* Reverse	5'-TCTGTCTTTGGCGTTGAGGTCTGC-3'
Human *SPARC* Forward	5'-GTGTGCAGCAATGACAACAAGACC-3'
Human *SPARC* Reverse	5'-GAATTCGGTCAGCTCAGAGTCCAG-3'
Human *ALDH1A3* Forward	5'-ATGGAAGACAAGGGGCTCTTCATC-3'
Human *ALDH1A3* Reverse	5'-AGAAGCCAACTTCAGGGCTTTGTC-3'
Human *SNAI2* Forward	5'-CGGACCCACACATTACCTTGTGTT-3'
Human *SNAI2* Reverse	5'-ATCAGAATGGGTCTGCAGATGAGC-3'
ChIP-qPCR for human *CCN1* (-0.3 kb) Forward	5'-CAAAGGTGCAATGGAGCCAGG-3'
ChIP-qPCR for human *CCN1* (-0.3 kb) Reverse	5'-GAGGCGCCGCGTGTTGCAG-3'
ChIP-qPCR for human *CCN1* (-0.85 kb) Forward	5'-CTTTGGGACTTGTTCCGAACACG-3'
ChIP-qPCR for human *CCN1* (-0.85 kb) Reverse	5'-TGACCGGGCAGCCACTGAAGC-3'
ChIP-qPCR for human *ALDH1A3* (-0.52 kb) Forward	5'-AGCAGGGCACGTGCGCAGC-3'
ChIP-qPCR for human *ALDH1A3* (-0.52 kb) Reverse	5'-CACATGCAGCCCACTCCCAG-3'
ChIP-qPCR for human *SPARC* (-0.67 kb) Forward	5'-CTTCCTCCTCTGTCGCCTCCTC-3'
ChIP-qPCR for human *SPARC* (-0.67 kb) Reverse	5'-GAGAAAAATGTGGCCACCCTCA-3'
ChIP-qPCR for human *SPARC* (-3.2 kb) Forward	5'-AAACTGCCAACGGCTAACAGCA-3'
ChIP-qPCR for human *SPARC* (-3.2 kb) Reverse	5'-CCAGGAACTCAGGCCAGTTCAA-3'

Table S2. shRNA or sgRNA sequences

	Target gene	Sequence (Sence)
shControl	non-target (SIGMA, Cat #SHC216)	GCGCGATAGCGCTAATAATTT
shBRD4 #1	NM_058243	GCUCAAGACACUAUGGAAACA
shBRD4 #2	NM_058243	GGUACCAAACACAACUCAAGC
shTAZ	NM_015472	ACGUUGACUUAGGAACUUU
sgTAZ	NM_015472	ATCCGAAGCCTAGCTCGTGG
sgYAP1	NM_001130145	GCATCAGATCGTGCACGTCCG